

## Coulomb drag in high Landau levels

I. V. Gomyi<sup>1,2</sup>, A. D. Mirlin<sup>1,2,3</sup>, and F. von Oppen<sup>3,4</sup><sup>1</sup>Institut für Nanotechnologie, Forschungszentrum Karlsruhe, 76021 Karlsruhe, Germany<sup>2</sup>Institut für Theorie der Kondensierten Materie,  
Universität Karlsruhe, 76128 Karlsruhe, Germany<sup>3</sup>Department of Condensed Matter Physics, Weizmann Institute of Science, Rehovot 76100, Israel<sup>4</sup>Institut für Theoretische Physik, Freie Universität Berlin, Am Müllke 14, 14195 Berlin, Germany  
(Dated: April 14, 2004)

Recent experiments on Coulomb drag in the quantum Hall regime have yielded a number of surprises. The most striking observations are that the Coulomb drag can become negative in high Landau levels and that its temperature dependence is non-monotonous. We develop a systematic diagrammatic theory of Coulomb drag in strong magnetic fields explaining these puzzling experiments. The theory is applicable both in the diffusive and the ballistic regimes; we focus on the experimentally relevant ballistic regime (interlayer distance smaller than the cyclotron radius  $R_c$ ). It is shown that the drag at strong magnetic fields is an interplay of two contributions arising from different sources of particle-hole asymmetry, namely the curvature of the zero-field electron dispersion and the particle-hole asymmetry associated with Landau quantization. The former contribution is positive and governs the high-temperature increase in the drag resistivity. On the other hand, the latter one, which is dominant at low  $T$ , has an oscillatory sign (depending on the difference in filling factors of the two layers) and gives rise to a sharp peak in the temperature dependence at  $T$  of the order of the Landau level width.

PACS numbers: 73.63.-b, 72.10.-d, 73.23.-b, 73.43.-f

## I. INTRODUCTION

Coulomb drag between parallel two-dimensional electron systems<sup>1,2</sup> has developed into a powerful probe of quantum Hall systems,<sup>3,4,5,6,7,8,9,10</sup> providing information which is complementary to conventional transport measurements. The drag signal is the voltage  $V$  developing in the open-circuit passive layer when a current  $I$  is applied in the active layer. The drag resistance (also known as transresistance) is then defined by  $R_D = V/I$ . As a function of interlayer spacing  $a$ , the interlayer coupling changes from weak at large spacings where it can be treated in perturbation theory, to strong at small spacings where it can result in states with strong interlayer correlations<sup>8,9</sup>. In the present paper we will be concerned with the regime of weak interlayer interaction.

In a simple picture of Coulomb drag, the carriers of the active layer transfer momentum to the carriers of the passive layer by interlayer electron-electron scattering. Due to the open-circuit setup, a voltage  $V$  develops in the passive layer, which balances this momentum transfer. The phase space for interlayer scattering is proportional to the temperature  $T$  in either layer predicting a monotonic temperature dependence  $R_D \propto T^2$  of the drag resistance. Moreover, the signs of the voltages in active and passive layer are expected to be opposite (the same) for carriers of equal (opposite) charge in the two layers.<sup>11</sup> It is conventional to refer to the sign resulting for like (unlike) charges as positive (negative) drag. It is worth emphasizing that, as the above considerations imply, the non-zero value of drag in the regime of weak interlayer interaction is entirely due to the violation of the particle-hole symmetry.

Remarkably, experiments show that Coulomb drag behaves very differently from these simple expectations when a perpendicular magnetic field  $B$  is applied such that the Fermi energy  $E_F$  is in a high Landau level,  $E_F = \hbar \omega_c (l - 1/2)$ . ( $\omega_c$  is the cyclotron frequency.) Several experiments<sup>5,7</sup> in the regime of weak interlayer coupling observed negative drag when the filling factors in the two layers are different. A more recent experiment<sup>10</sup> also reveals a non-monotonic dependence on temperature. While the drag resistivity shows a quadratic temperature dependence at sufficiently high temperatures, where drag is always positive, an additional peak develops at low temperatures which can have both a positive or a negative sign depending on the filling-factor difference between the two layers.

Early theoretical work<sup>12</sup> on Coulomb drag in a magnetic field in the limit of high Landau levels showed that the magnetic field may strongly enhance the Coulomb drag, as indeed observed experimentally. On the other hand, the calculation of Ref. 12, as well as of a later paper,<sup>13</sup> results in a strictly positive transresistivity, in contradiction with the oscillatory sign found in recent experiments. As we discuss in detail below, a general formula for the drag resistivity obtained in Ref. 12, which looks like a natural generalization of the zero- $B$  result<sup>11,15,16</sup> and also served

Permanent address

as a starting point for Ref. 13, misses an important contribution. This strongly restricts the range of validity of the results of Refs. 12,13, making them inapplicable under typical experimental conditions. More recent work<sup>14</sup> showed that Landau-level quantization can lead to sign changes in drag. However, the results obtained in Ref. 14 suggested that unlike the experimental observation, negative drag should be observed for equal filling factors in the two layers. The temperature dependence of the drag resistivity was not studied in 14.

In this paper, we present a systematic study of Coulomb drag in the limit of high Landau levels. We focus on the experimentally relevant limit of well-separated Landau levels (LLs) in which the LL broadening is small compared to the LL spacing  $\hbar\omega_c$ . Our starting point is the diagrammatic Kubo formulation of Coulomb drag<sup>15,16</sup> for weak interlayer interaction. Disorder is included at the level of the self-consistent Born approximation<sup>17</sup> (SCBA) which becomes exact in the limit of high Landau levels<sup>18</sup>.

Our results are in good agreement with the experimental observations. We find that at high temperatures, the leading contribution to Coulomb drag is due to the breaking of particle-hole symmetry by the quadratic dispersion of the electrons. This contribution which is analogous to the conventional contribution to drag discussed above, always has a positive sign and depends on temperature as  $T^2$ . At temperatures  $k_B T \ll \hbar\omega_c$ , we find that the dominant contribution arises from the breaking of particle-hole symmetry due to the Landau-level structure. This contribution gives rise to a peak in the temperature dependence and can take on both positive and negative signs, depending on the filling-factor difference of the two layers. In particular, the sign is negative for equal filling factors in the diffusive regime where the interlayer distance  $a$  is larger than the cyclotron radius  $R_c$ , as was found in Ref. 14. We find, however, that this sign becomes negative in the experimentally relevant ballistic regime ( $a$  small compared to  $R_c$ ), in agreement with experiment.

This paper is organized as follows. Sec. II briefly summarizes the pertinent background on the Kubo approach to Coulomb drag as well as on the self-consistent Born approximation. In Sec. III, we present the diagrammatic calculation of the triangle vertex entering the expression for the drag conductivity, for well-separated LLs, both in the diffusive and in the ballistic regime of momenta. In Sec. IV, we collect the relevant results for the screened interlayer interaction. These building blocks are used in Sec. V to compute the drag resistivity. In this section, we also compare our results with experiment. Finally, Sec. VI contains a summary of our results and a discussion of prospects for future research. In what follows, we set  $\hbar = k_B = 1$ :

## II. BACKGROUND

### A. Drag

Our considerations are based on the Kubo approach to Coulomb drag<sup>15,16</sup> which expresses the drag conductivity  $D_{ij}^D(Q; \omega)$  in terms of a current-current correlation function,

$$D_{ij}^D(Q; \omega) = \frac{1}{S} \int_0^{\infty} dt e^{i\omega t} \langle [j_i^{(1)y}(Q; t); j_j^{(2)}(Q; 0)] \rangle \quad (1)$$

where  $i, j$  label the components of the drag conductivity tensor,  $Q; \omega$  denote the wave vector and frequency of the applied field,  $S$  is the area of the sample, and  $j_i^{(l)}$  denotes the  $i$ th component of the current operator in the  $l$ th layer. The dc drag conductivity follows by taking the limit

$$D_{ij}^D = D_{ij}^D(Q = 0; \omega \rightarrow 0) \quad (2)$$

When computing the retarded correlation function appearing in Eq. (1) within the Matsubara technique, the leading diagrams in the limit of weak (screened) interlayer interaction  $U(q; \omega)$  are shown in Fig. 1. Analytically, these diagrams are given by the expression

$$D_{ij}^D(i_k) = \frac{e^2 T}{2k_S} \sum_{q; \omega_n} X_i^{(1)}(q; i_n + i_k; i_n) X_j^{(2)}(q; i_n; i_n + i_k) U(q; i_n + i_k) U(q; i_n) \quad (3)$$

Here,  $\omega_n$  and  $\omega_k$  denote bosonic Matsubara frequencies and the vector  $X^{(l)}(q; i_n; i_m)$  is the triangle vertex of layer  $l$  as defined by the diagrams in Fig. 2. Neglecting intralayer interactions, it takes the analytical form

$$X(q; i_n; i_m) = T \sum_k \text{tr} G(i_k) e^{iq \cdot r} G(i_k + i_m) v G(i_k + i_n) e^{-iq \cdot r} + G(i_k) e^{iq \cdot r} G(i_k - i_n) v G(i_k - i_m) e^{-iq \cdot r} \quad (4)$$

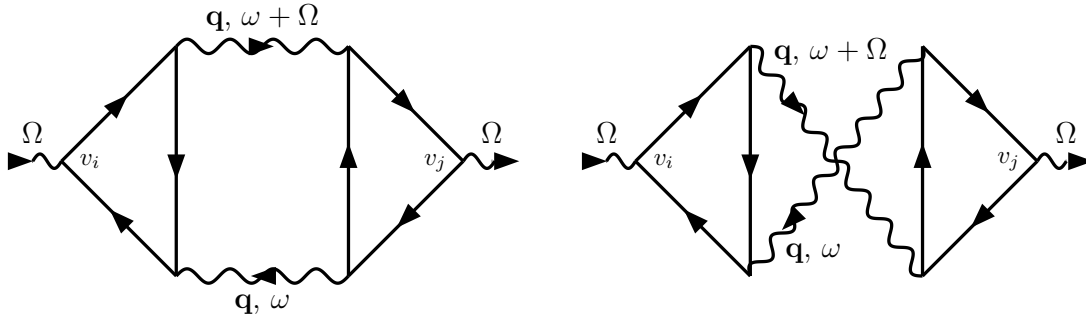


FIG. 1: The diagrams contributing to the drag conductivity to leading order in the interlayer interaction  $U(\mathbf{q};!)$  (wavy lines). The full lines represent the electron Green function. The external vertices labelled by the velocity operator  $v_i$  are vector (current) vertices while the internal vertices are scalar (density) vertices.

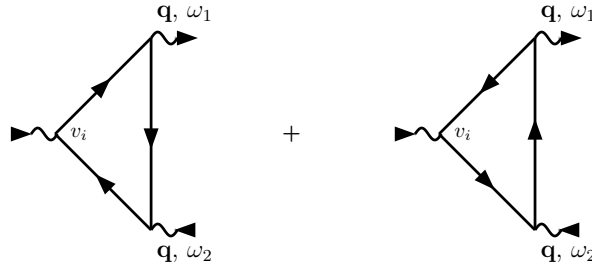


FIG. 2: Diagrams defining the triangle vertex  $\Gamma(\mathbf{q};!_1;!_2)$ .

where  $G$  denotes the Green function (for a particular realization of the disorder potential),  $\omega_k$  is a fermionic Matsubara frequency, and  $v$  represents the velocity operator. The vertex should be averaged over realizations of disorder, as will be discussed in Sec. II B.

Summing over the Matsubara frequency  $\omega_n$ , performing the analytical continuation to a real frequency  $\omega$ , and finally taking the limit  $\omega \rightarrow 0$  yields for the dc drag conductivity<sup>15,16</sup>

$$\chi_{ij}^D = \frac{e^2}{16 T S} \sum_{\mathbf{q}} \sum_{\omega} \frac{d!}{\sinh^2(\omega/2T)} \Gamma_i^{(1)}(\mathbf{q};! + i0;! - i0) \Gamma_j^{(2)}(\mathbf{q};! - i0;! + i0) \mathcal{J}(\mathbf{q};!) \quad (5)$$

In the sequel, we will use a short-hand notation,  $\Gamma(\mathbf{q};!) = \Gamma(\mathbf{q};! + i0;! - i0)$ . Note that the Onsager relation  $\chi_{ij}^{12}(\mathbf{B}) = \chi_{ji}^{21}(\mathbf{B})$  implies, in combination with (5), that  $\Gamma(\mathbf{q};! - i0;! + i0; \mathbf{B}) = \Gamma(\mathbf{q};! + i0;! - i0; \mathbf{B})$ .

The experimentally measured drag resistivity can be expressed via the drag conductivity as

$$\rho_{ij}^D = \frac{\chi_{ik}^{(1)}}{\chi_{kl}^{(2)}} \rho_{lj}^{(2)}; \quad (6)$$

where  $\rho_{ik}^{(1;2)}$  are the resistivities of the layers. Note that the minus sign corresponding to the standard tensor inversion is absent in this expression, according to the conventional definition of the drag resistivity. This definition yields a positive transresistivity in the absence of a magnetic field.

The triangle vertex  $\Gamma(\mathbf{q};!)$  is obtained by analytic continuation of (4), see Appendix A for detail. The result has the form  $\Gamma = \Gamma^{(a)} + \Gamma^{(b)}$  with the two contributions

$$\begin{aligned} \Gamma^{(a)}(\mathbf{q};!) &= \frac{d}{4 i} \tanh \frac{\omega + !}{2T} \\ &\text{tr } v G^+(\omega + !) e^{i\mathbf{q}\cdot\mathbf{r}} G^+(\omega) e^{i\mathbf{q}\cdot\mathbf{r}} G^+(\omega + !) v G(\omega + !) e^{i\mathbf{q}\cdot\mathbf{r}} G(\omega) e^{i\mathbf{q}\cdot\mathbf{r}} G(\omega + !) + (!; \mathbf{q}; !; \mathbf{q}); \quad (7) \\ \Gamma^{(b)}(\mathbf{q};!) &= \frac{d}{4 i} \left( \tanh \frac{\omega + !}{2T} - \tanh \frac{\omega}{2T} \right) \\ &\text{tr } v G(\omega + !) e^{i\mathbf{q}\cdot\mathbf{r}} G(\omega) G(\omega) e^{i\mathbf{q}\cdot\mathbf{r}} G^+(\omega + !) + (!; \mathbf{q}; !; \mathbf{q}); \quad (8) \end{aligned}$$

Here,  $G(\omega)$  denotes the advanced/retarded Green function and  $\mu$  is the chemical potential. Note that at zero magnetic field only  $\Gamma^{(b)}$  survives,<sup>15</sup> whereas  $\Gamma^{(a)}$  containing products of three advanced or three retarded Green functions is

zero. By contrast, in strong B both <sup>(a)</sup> and <sup>(b)</sup> should be retained. Most importantly, we will show below that in the ballistic limit there is a cancellation between <sup>(a)</sup> and <sup>(b)</sup> in the leading order.

For small  $l$ , the expressions for  $\chi(q; l)$  simplify to

$$\chi^{(a)}(q; l) = \frac{l}{2} \frac{1}{i} \text{tr} \left[ v G^+ (r) e^{iqr} G^+ (r) e^{iqr} G^+ (r) \right] \quad (9)$$

$$\chi^{(b)}(q; l) = \frac{l}{i} \text{tr} \left[ v G (r) e^{iqr} [G (r) \cdot \hat{G} (r)] e^{iqr} G^+ (r) \right] \quad (10)$$

For well-separated LLs, this approximation holds as long as  $l$  is small compared to the width of the LL. It is also useful to note that  $\chi^{(a)}(q; l)$  can be expressed as

$$\chi^{(a)}(q; l) = \frac{l}{2} r_q \text{Im} \text{tr} \left[ e^{iqr} G^+ (r) e^{iqr} G^+ (r) \right]; \quad (11)$$

which shows that  $\chi^{(a)}(q; l)$  gives only a longitudinal contribution (parallel to  $q$ ) to  $\chi(q; l)$ .

### B. Impurity diagram technique in high Landau levels (SCBA)

In this subsection, we discuss the averaging over the random potential of impurities. We assume white-noise disorder, characterized by zero mean,  $\langle U(r) \rangle = 0$ , and by the correlation function

$$\langle U(r) U(r') \rangle = \frac{1}{2} \delta(r - r');$$

where  $\rho_0 = m^{-2}$  denotes the zero-B density of states per spin and  $\rho_0$  the zero-B elastic scattering time. We perform the averaging in the self-consistent Born approximation (SCBA). This approximation, which neglects diagrams with crossing impurity lines, can be shown to give the leading contribution when the Fermi energy  $E_F$  is in a high LL with LL index  $N \gg 1$ .<sup>18</sup> Strictly speaking, the disorder potential in the experimental samples is expected to be correlated on the scale of the distance of the two-dimensional electron layer from the donor layer. However, we find that the experimental observation can already be understood when considering white-noise disorder and that a finite correlation length of disorder does not qualitatively change our conclusions.<sup>19</sup>

Within the SCBA for well-separated Landau levels,<sup>17</sup> the impurity average of the Green function, denoted by  $G_n(r)$ , is diagonal in the LL basis  $j, k$  in the Landau gauge and takes the expression

$$G_n(r) = \frac{1}{E_n - i0^+} \quad (12)$$

with the LL energies  $E_n = \hbar \omega_c (n + 1/2)$ . For energies within a Landau level, the self-energy is given by

$$\Sigma_n(r) = \frac{1}{2} \rho_0 \int d^2r' \left[ \frac{1}{E_n - i0^+ - \hbar \omega_c} \right]^2 g(r - r'); \quad (13)$$

Here, the LL index  $n$  is chosen such that  $j = n$ ,  $j + 1 < n + 1$ . The LL broadening can be expressed in terms of the zero-field scattering time  $\tau_0$  as

$$\tau_0^{-1} = 2 \rho_0 \omega_c; \quad (14)$$

The density of states is

$$\rho_n = \frac{1}{2} \rho_0 \left[ \frac{1}{E_n - i0^+ - \hbar \omega_c} \right]^2 \quad (15)$$

with the elastic scattering time

$$\tau_n = \left[ \frac{1}{E_n - i0^+ - \hbar \omega_c} \right]^{-2}; \quad (16)$$

Here,  $\lambda = (1/eB)^{1/2}$  denotes the magnetic length.

In principle, disorder leads to vertex corrections of both the vector and the scalar vertices of the triangle diagram. However, for white-noise disorder there are no vertex corrections of the vector vertex. The vertex corrections of the scalar vertices generally involve impurity ladders (cf. Fig. 3) and turn out to be independent of the LL indices  $n$  and  $n'$ .<sup>21</sup>

$$\chi_{nk, n'k'}^{(a)}(r, r'; q) = \chi^{(a)}(q; l) \rho_n \rho_{n'} \delta_{nk, n'k'}; \quad (17)$$

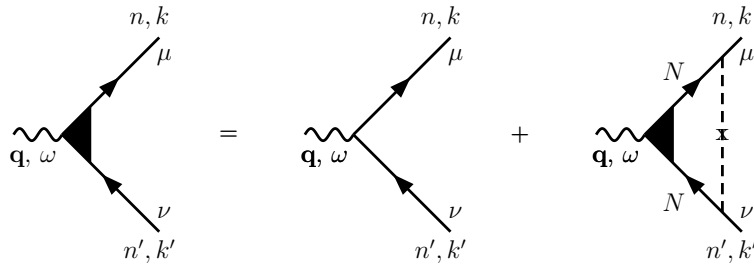


FIG. 3: Diagrammatic representation of the equation for the vertex corrections  $\Gamma_{nk;n^0k^0}^{++}(\omega; \mathbf{q})$  (full triangle at vertex) of the scalar (density) vertices in the SCBA. Dashed lines represent impurity scattering. We also indicate that for well-separated LLs, the internal Green functions in the right-most diagram should be evaluated in the valence LL  $N$  which can differ from the LL labels  $n; n^0$  of the external Green functions.

Here, the indices  $++$  indicate the type of Green functions involved in the vertex. In the limit of well-separated Landau levels, one finds the explicit expressions for the vertex corrections at  $\omega = 0$

$$\Gamma_{nk;n^0k^0}^{++}(\mathbf{q}; 0) = \frac{1}{1 - J_0^2(qR_c) - 2\gamma^2} \quad (18)$$

$$\Gamma_{nk;n^0k^0}^{+}(\mathbf{q}; 0) = \frac{1}{1 - J_0^2(qR_c)} \quad (19)$$

where  $J_n(z)$  denotes the Bessel functions. The derivation of these expressions is reviewed in Appendix B.

For later reference, we also collect relevant matrix elements between LL eigenstates  $jki$  in the Landau gauge  $A = B(0; x)$ . The vector vertex involves the matrix elements

$$\langle nk | j_x | jn^0 k^0 \rangle_i = \frac{i}{m} \frac{p}{\sqrt{2}} \left[ \frac{p}{n} \delta_{n, n^0+1} - \frac{p}{n+1} \delta_{n, n^0-1} \right] \quad (20)$$

$$\langle nk | j_y | jn^0 k^0 \rangle_i = \frac{1}{m} \frac{p}{\sqrt{2}} \left[ \frac{p}{n} \delta_{n, n^0+1} + \frac{p}{n+1} \delta_{n, n^0-1} \right] \quad (21)$$

In the limit of high Landau levels,  $n \gg N \gg 1$ , one can use quasiclassical approximations for these matrix elements, namely  $\langle nk | j_x | jn^0 k^0 \rangle_i \approx i_{kk^0} v_F = 2$  and  $\langle nk | j_y | jn^0 k^0 \rangle_i \approx 1 k^0 i'_{kk^0} v_F = 2$ , with the Fermi velocity  $v_F$ .

The scalar vertex involves the matrix element

$$\langle nk | j^{iqx} | jn^0 k^0 \rangle_i = \alpha_{y; k} \frac{2^{n^0} n!}{n^0} \exp\left[\frac{1}{4} q^2 r^2 - \frac{i}{2} q_x (k + k^0) r^2\right] [(q_y + i q_x)]^n L_{n^0}^{n-n^0}(q^2 r^2) \quad (n > n^0); \quad (22)$$

where  $L_m^n$  is the associated Laguerre polynomial. The expression for the matrix element for  $n < n^0$  can be obtained from (22) by complex conjugation with the replacement  $q \rightarrow q^*$ ,  $n \rightarrow n^0$ . Since the characteristic LL indices are large,  $n; n^0 \gg 1$ ;  $j; jn^0$ , and relevant momenta are small compared to the Fermi momentum,  $q \ll k_F$ , Eq. (22) can be simplified by using the quasiclassical approximation,

$$\langle nk | j^{iqx} | jn^0 k^0 \rangle_i \approx \alpha_{y; k} i^n \frac{1}{n^0} e^{-i q (n - n^0) r^2} e^{i q_x (k + k^0) r^2} J_{n - n^0}(q R_c^{(n)}); \quad (23)$$

where  $q$  is the polar angle of  $\mathbf{q}$ ,  $R_c^{(n)} = \sqrt{\frac{p}{2n+1}}$  is the cyclotron radius of the  $n$ -th LL, and  $m = (n + n^0) = 2$ . For most of the calculations below, the dependence of the cyclotron radius on the LL index in the vicinity of the Fermi level will be immaterial, and we will drop the corresponding superscript and simply write  $R_c$ . The  $n$ -dependence of  $R_c$  will, however, be crucial for the evaluation of the contribution to the drag related to the curvature of the electron spectrum, see Sec. III C 3. In view of the rotational invariance of  $\Gamma(\mathbf{q}; 0)$ , it is sufficient to calculate it for a certain direction of the wave vector  $\mathbf{q}$ . Choosing  $\mathbf{q}$  to point along the positive  $x$ -axis, we simplify (23) to the form

$$\langle nk | j^{iqx} | jn^0 k^0 \rangle_i \approx \frac{i}{m} \frac{1}{n^0} e^{i q k^0 r^2} J_{n - n^0}(q R_c); \quad (24)$$

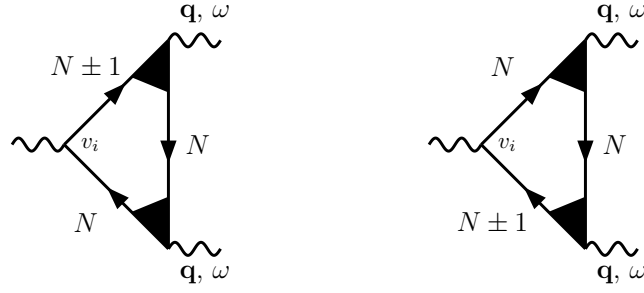


FIG. 4: The diagrams contributing to the triangle vertex in SCBA to leading order in the limits of well-separated Landau levels  $\omega_c \ll \omega$  and large  $N$ .

### III. TRIANGLE VERTEX $\chi(q; \omega)$

#### A. Leading order

We now turn to an evaluation of the disorder-averaged triangle vertex  $\chi(q; \omega)$  for well-separated Landau levels,  $\omega_c \ll \omega$ ; in the limit in which the Fermi energy is in a high Landau level,  $N \gg 1$ . The relevant diagrams are shown in Fig. 4. We begin by considering the low-temperature limit,  $\omega \gg T$ :

In the limit under consideration, the calculation is simplified as follows. Very generally for white-noise disorder, there are no vertex corrections of the vector vertex. By contrast, vertex corrections of the scalar vertices have to be retained. To leading order in  $\omega_c \ll \omega$ , two of the three Green functions in Eqs. (9) and (10) should be evaluated in the  $N$ th Landau level in which the Fermi energy is situated. Since the velocity operator has matrix elements only between states in neighboring Landau levels, one of the Green functions adjacent to the vector vertex must be taken in Landau level  $N \pm 1$ . This is illustrated in Fig. 4.

We first consider the contribution  $\chi^{(a)}(q; \omega)$ . In this case, it is most convenient to start from the simplified expression in Eq. (11) in which to leading order in  $\omega_c \ll \omega$ , both remaining Green functions can be evaluated in Landau level  $N$ . Using the identity  $\text{tr}_q [J_0(qR_c)]^2 = 2\hat{q}R_c J_0(qR_c)J_1(qR_c)$  (with  $\hat{q} = q = \omega$ ), one obtains

$$\chi^{(a)}(q; \omega) = 2\hat{q} \frac{R_c}{2v_F} J_0(qR_c)J_1(qR_c) \frac{1}{2i} \text{f} [G_N^{++}]^2 \text{f} G_N \text{f}^2 g; \quad (25)$$

where  $\text{f} \chi(q; \omega)$  and the factor 2 accounts for the spin degeneracy. The calculation for  $\chi^{(b)}(q; \omega)$  in Eq. (10) yields

$$\chi^{(b)}(q; \omega) = 2\hat{q} \frac{R_c}{2v_F} J_0(qR_c)J_1(qR_c) \frac{1}{2i} [G_N^{++} + G_N^+][G_N^+ + G_N]: \quad (26)$$

Summing both contributions, one obtains

$$\chi(q; \omega) = \hat{q} \frac{4R_c}{2v_F} J_0(qR_c)J_1(qR_c) \text{Re} [G_N^{++}] \text{Im} [G_N^{++}]: \quad (27)$$

For arbitrary  $T; \omega < \omega_c$ , this contribution takes the form<sup>22</sup>

$$\chi(q; \omega) = \hat{q} \frac{8R_c}{2v_F} \frac{J_1(qR_c)}{J_0(qR_c)} \int_0^1 d \tanh \frac{\omega}{2T} \tanh \frac{\omega}{2T} \text{Re} [G_N^{++}(q; \omega)] \text{Im} [G_N^{++}(q; \omega)]: \quad (28)$$

Since the interlayer interaction is suppressed at large momenta  $q$  by a factor  $e^{-qa}$ , where  $a$  is the interlayer distance, the drag conductivity (5) is governed by momenta  $q < 1/a$ . Depending on the relation between  $a$  and the cyclotron radius  $R_c$ , one distinguishes between the diffusive ( $a > R_c$ ) and the ballistic ( $a < R_c$ ) regimes. While in the former case, only "diffusive" momenta ( $qR_c < 1$ ) are relevant, in the latter case both "ballistic" ( $qR_c < 1$ ) and diffusive momenta contribute to the drag conductivity (5). Experimentally, when the transresistivity is measured in moderately strong magnetic fields (i.e. in high Landau levels), the condition  $R_c > a$  is typically satisfied. For this reason, we mainly concentrate on the ballistic regime in this paper. In Secs. IIIB and IIIC we will calculate the triangle vertex  $\chi(q; \omega)$  in the diffusive and ballistic ranges of momenta, respectively. These results will be used in Sec. V for the calculation of the drag resistivity.

### B. Diffusive momenta, $qR_c \ll 1$

In the diffusive range of momenta,  $qR_c \ll 1$ , we can expand the Bessel functions in the expressions for the vertex corrections, Eqs. (18) and (19). Due to the singular behavior of the vertex correction  $\chi^{++}$  at small momenta  $q$ , we have  $\chi^{++} \sim \chi^{++}$ ; , so that only the contribution proportional to  $\chi^{++}$  should be retained in (27). This yields

$$\chi(q;!) = \frac{4! R_c (qR_c)}{2^2 2^2} \frac{2}{(qR_c)^2} \frac{E_N}{[2 - (E_N)^2]^{1/2}}; \quad (29)$$

More generally, at small momenta one should also take into account the frequency dependence of  $\chi^{++}$ , which has the structure of a diffusion pole,

$$\chi^{++}(q;!) = \frac{1}{D(\omega) D(\omega) \tilde{q}^2 i!}; \quad (30)$$

where  $D(\omega) = R_c^2 \omega^2$  is the (energy-dependent) diffusion constant in a strong magnetic field. Eq. (29) is then generalized to

$$\chi(q;!) = \frac{4! q R_c^2}{2^2 2^2} \frac{D(\omega) q^2}{D(\omega) q^2 \tilde{q}^2 + i!^2} (\omega, E_N); \quad (31)$$

This result can be recast in the form ( $n_e$  is the electron concentration)

$$\chi_{ij}(q;!) = 2 \frac{d_{ij}}{d(n_e)} \chi_{ij} \text{Im}(q;!) + 2 \frac{d_{xx}}{d(n_e)} \chi_{xx} \text{Im}(q;!); \quad (32)$$

which allows for a simple interpretation as a nonlinear susceptibility.<sup>14,20</sup> This rewriting of Eq. (31) uses the result<sup>17</sup>

$$\chi_{xx} = \frac{e^2}{2} N \frac{1}{2} \frac{(E_N)^2}{2} \quad (33)$$

for the diagonal conductivity in SCBA ( $d_{xx} = dn_e$ ,  $d_{xy} = dn_e$  for separated LLs) and

$$\chi(q;!) = 2 \frac{D(\omega) q^2}{D(\omega) q^2 i!}; \quad (34)$$

for the polarization operator in the diffusive limit. It is worth emphasizing that the diffusive result in Eq. (31) arises from (b) only, since the other contribution (a) does not contain the vertex correction  $\chi^{++}$ . Note that the authors of Ref. 12 failed to obtain the leading diffusive contribution (31), (32), because of an incorrect treatment of vertex corrections<sup>21,22</sup>. For the same reason, they missed the  $O(1=qR_c)$  contribution [Eq. (36) below] which becomes important in the ballistic regime, as we are going to discuss.

### C. Ballistic momenta, $qR_c \gg 1$

#### 1. Cancellation of leading contribution and the $O(1=qR_c)$ contribution from vertex corrections

In the leading order in the ballistic range of momenta,  $qR_c \gg 1$ , the vertex corrections in Eqs. (18) and (19) can be neglected,

$$\chi^{++}(q;!) \approx \chi^{++}(q;!) \approx 1; \quad (35)$$

Inserting this into Eq. (27) for the triangle vertex  $\chi(q;!)$ , we immediately see that the triangle vertex vanishes to this order. We emphasize that (a) and (b) do not vanish separately but rather cancel each other in the leading order.

Thus, to obtain a non-zero answer for  $\chi(q;!)$  from Eq. (27), we need to consider the vertex corrections in Eqs. (18) as (19) in next-to-leading order in  $qR_c$ . In this way, one finds from Eq. (27)

$$\chi^{(1=qR_c)}(q;!) = \frac{64! R_c}{2^2 2^2} \frac{(E_N)^2 [2 - (E_N)^2]^{3/2}}{6} J_1(qR_c) J_0^3(qR_c); \quad (36)$$

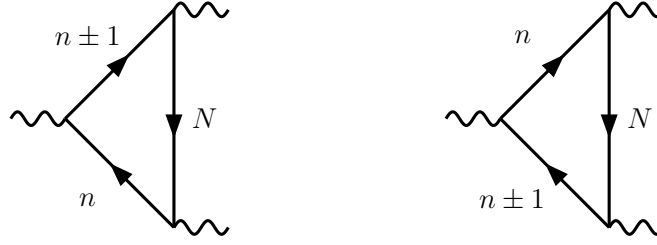


FIG. 5: Diagram contributing to corrections of order  $\omega_c$  to the triangle vertex. Here both Green function adjacent to the vector vertex should be evaluated in Landau levels different from  $N$ .

Here, we introduced a superscript on  $(q; !)$  in order to distinguish this contribution from other contributions computed below. At finite  $T$  and  $\omega_c$  (assuming  $T; ! < \omega_c$ ), we find

$$\begin{aligned}
 {}^{(1=qR_c)}(q; !) &= \hat{q} \frac{16! R_c}{2^2} J_1(qR_c) J_0^3(qR_c) \int_0^1 d \tanh \frac{\omega_c}{2T} \tanh \frac{\omega_c}{2T} \\
 &\text{Re } 1 \frac{(\omega_c - E_N)^2}{2} {}^{1=2} \text{Re } 1 \frac{(\omega_c - E_N)^2}{2} {}^{1=2} \\
 &\frac{\omega_c - E_N}{1} \frac{(\omega_c - E_N)^2}{2} + \frac{\omega_c - E_N}{1} \frac{(\omega_c - E_N)^2}{2} : \quad (37)
 \end{aligned}$$

The contribution (36) to  $(q; !)$  has been obtained in leading order in the limit  $\omega_c \ll 1$  and  $q=k_F \ll 1$  and in next-to-leading order in  $qR_c \ll 1$ . Thus, we are also forced to consider separately next-to-leading order corrections in the parameters  $\omega_c \ll 1$  and  $q=k_F \ll 1$ , with the other two parameters kept in leading order.

Before we turn to these calculations, we briefly remark that the leading-order cancellation in the ballistic regime was missed in Ref. 14 since the contribution from  $^{(a)}$  was overlooked. The results obtained there for the diffusive regime remain valid since in this case  $^{(a)}$  is negligible compared to  $^{(b)}$ , see Sec. IIIB.

## 2. Contributions of order $\omega_c$

In this section, we consider the first corrections to the leading order in  $\omega_c$  to the triangle vertex  $(q; !)$ , while working to leading order in the ballistic limit  $qR_c \ll 1$  for high Landau levels  $N \gg 1$ . While such corrections are of higher order in the small parameter  $\omega_c$ , this smallness may be compensated by a large factor  $qR_c$  since it turns out that in this case there is no cancellation between  $^{(a)}$  and  $^{(b)}$ .

Corrections of order  $\omega_c$  arise from two sources: (i) The Green functions adjacent to the current vertex are both evaluated in Landau levels different from  $N$ . (Note that the Green function between the scalar vertices must still be evaluated in the  $N$ th Landau level because  $G_n^+ G_n = \omega_c^2$  for  $n \notin N$ .) This contribution is depicted in Fig. 5. (ii) The diagrams in Fig. 4 can be evaluated more accurately, keeping corrections in  $\omega_c$ , which arise from keeping the self-energy parts of the Green functions of Landau levels  $N \gg 1$ . Note that we may now neglect vertex corrections at the scalar vertices because we consider the leading order in  $qR_c \ll 1$ .

Details of this calculation are presented in Appendix C. Here we only state the results. The contribution (i) vanishes for both  $^{(a)}$  and  $^{(b)}$ . The contribution (ii) turns out to still give a vanishing contribution to the longitudinal triangle vertex, due to the cancellation between  $^{(a)}$  and  $^{(b)}$  described above. However, the transverse contribution to  $^{(b)}$  no longer vanishes when considering corrections in  $\omega_c$ . In this way, we obtain the contribution

$${}^{(\omega_c)}(q; !) = \hat{q} \frac{16! R_c}{2^2} \frac{(E_N)^2 (E_N)^2}{\omega_c^4} J_0(qR_c) J_1(qR_c) \quad (38)$$

to the triangle vertex.

As we will see below, the  $\omega_c$  contribution is of crucial importance for understanding the experimental findings. We mention that this term was lost in Ref. 12 (in addition to the  $1=qR_c$  contribution missing there because of an inaccurate treatment of vertex corrections) in the course of the so-called "triangles-to-bubbles" transformation. Specially, in Ref. 12 the self-energy in the Green functions connected by the current vertex was neglected compared to the cyclotron frequency, which obviously misses corrections of order of  $\omega_c$ .

Eq. (38) is derived in the low-temperature limit, when  $T; ! \ll \omega_c$ . To analyze the temperature dependence of the drag, we will need the  $\omega_c$ -contribution also at higher temperatures. We end for arbitrary relations between  $T$  and



## IV. SCREENED INTERLAYER INTERACTION

In this section, we summarize the results for the screened interlayer interaction<sup>15</sup>

$$U_{12}(\mathbf{q};!) = \frac{V_{12}(\mathbf{q})}{[1 + V(\mathbf{q}) \chi_1(\mathbf{q};!)] [1 + V(\mathbf{q}) \chi_2(\mathbf{q};!)]} V_{12}^2(\mathbf{q}) \chi_1(\mathbf{q};!) \chi_2(\mathbf{q};!) : \quad (47)$$

Here,  $V(\mathbf{q}) = 2e^2/q$  denotes the bare intralayer interaction and  $V_{12}(\mathbf{q}) = V(\mathbf{q})e^{-qa}$  is the bare interlayer interaction,  $a$  denotes the distance between the layers. The polarization operator of layer 1 is denoted by  $\chi_1(\mathbf{q};!)$ . For  $q$  small compared to the Thomas-Fermi screening wave vectors  $\chi_{0;l} = 4e^2 \chi_{0;l}$  ( $l = 1, 2$  labels the layer and  $\chi_{0;l}$  denotes the zero-field density of states per spin of layer  $l$ ), this can be approximated as

$$U_{12}(\mathbf{q};!) \approx \frac{e^2 q}{\chi_{0;1} \chi_{0;2} \sinh(qa)} \frac{\chi_{0;1}}{\chi_1(\mathbf{q};!)} \frac{\chi_{0;2}}{\chi_2(\mathbf{q};!)} : \quad (48)$$

In the random-phase approximation, the polarization operator in a strong magnetic field has the form

$$\begin{aligned} \chi(\mathbf{q};!) = & \frac{1}{\chi} \sum_{n,m} J_{n-m}^2(qR_c) \sum_{l=1}^Z \frac{d}{2i} n_F(\epsilon_l) [G_n^+(\epsilon_l +!) G_m^+(\epsilon_l) + G_n^+(\epsilon_l) G_m^+(\epsilon_l)] \\ & + G_n^+(\epsilon_l) G_m^+(\epsilon_l) + G_n^+(\epsilon_l) G_m^+(\epsilon_l) ; \end{aligned} \quad (49)$$

where  $n_F(\epsilon) = 1/(1 + \exp[(\epsilon - \mu)/T])$ ,  $\mu = \mu_0 \tanh[(\epsilon - \mu_0)/2T]$  is the Fermi distribution function and we have used the quasiclassical approximation for matrix elements (24).

We turn now to a brief summary of results for  $\chi(\mathbf{q};!)$  in various relevant domains of momentum and frequency. Some of these results can be found in Ref. 13; we reproduce them here for the sake of completeness. The polarization operator in the diffusive regime of momentum (and at  $T \ll \mu$ ) was already given in Eq. (34). In the ballistic regime  $qR_c \gg 1$ , the expression (49) can be simplified by neglecting the scalar vertex corrections,

$$\chi(\mathbf{q};!) = \frac{1}{\chi} \sum_{n,m} J_{n-m}^2(qR_c) \sum_{l=1}^Z \frac{d}{2i} n_F(\epsilon_l) [G_n^+(\epsilon_l +!) + G_n^+(\epsilon_l)] \text{Im} G_m^+(\epsilon_l); \quad (50)$$

For low temperature and frequency,  $! \ll T$ , the real part of the polarization operator (50) takes the form

$$\text{Re} \chi(\mathbf{q};!) = 2\chi_{0;1} + 2\chi_{0;2} \frac{8!}{3} J_0^2(qR_c) \sum_{l=1}^Z \frac{(\epsilon_N - \epsilon_l)^2}{2} \quad (51)$$

Here, the first term<sup>23</sup> arises from Landau levels with  $n \notin m$ , while the second term represents the contribution of the  $N$ th LL ( $n = m = N$ ). The intra-LL (second) term contains an additional energy factor  $\frac{4}{3} [(\epsilon_N - \epsilon_l)^2 = 2]$  compared to the case of diffusive momentum, which is due to the suppression of vertex corrections at high momentum. The imaginary part of the polarization operator for  $! \ll T$  has the form

$$\text{Im} \chi(\mathbf{q};!) = 2\chi_{0;1} \frac{4!}{2} J_0^2(qR_c) \sum_{l=1}^Z \frac{(\epsilon_N - \epsilon_l)^2}{2} : \quad (52)$$

A comparison with Eq. (51) shows that  $\text{Im} \chi \ll \text{Re} \chi$  in this regime.

It follows from Eq. (51) that there is an additional wavevector scale  $qR_c \approx \mu_c$  in the ballistic regime, where the behavior of  $\text{Re} \chi$  changes. Specially, for  $q \approx \mu_c = R_c$  the polarization operator (and hence screening) is due to the contribution of the  $N$ -th Landau level, while at larger  $q$  it is due to Landau levels with  $n \notin N$ . Only in the latter case, we recover

$$\chi(\mathbf{q};!) \approx 2\chi_{0;1} \quad (53)$$

and thus the standard  $B = 0$  form of screening. When the temperature is large compared to the Landau level broadening,  $T \approx \mu_c$ ; Eqs. (34), (52), and the second term of (51) are effectively multiplied by factors  $\approx T$  due to thermal averaging. In this case, the real part of  $\chi(\mathbf{q};!)$  takes its zero-B form under the weaker condition  $qR_c \approx \mu_c = T$ . This follows from the expression

$$\text{Re} \chi(\mathbf{q};!) = 2\chi_{0;1} + 2\chi_{0;2} \frac{2!}{T} J_0^2(qR_c) \sum_{l=1}^Z \frac{!}{2} \cosh^{-2} \frac{\epsilon_N - \epsilon_l}{2T} : \quad (54)$$

Here we defined the function

$$Q(x) = \int_{-1}^1 dz z (1-z^2)^{1/2} z \frac{\text{sgn}(z+2x)}{2} \text{Re}[(z+2x)^2 - 1]^{1/2} - \int_{-1}^1 dz z (1-z^2)^{1/2} z \frac{\text{sgn}(z-2x)}{2} \text{Re}[(z-2x)^2 - 1]^{1/2} : \quad (55)$$

The imaginary part for  $T \ll \omega_c$  reads

$$\text{Im}(q;!) = 2 \int_0^1 \frac{J_0^2(qR_c)}{T} \frac{!}{2} H\left(\frac{!}{2} \cosh^{-2} \frac{E_N}{2T}\right) ; \quad (56)$$

where  $H(x)$  is a dimensionless function representing the overlap of two Landau bands,

$$H(x) = \int_{-1}^1 dz \text{Re} \left[ \frac{1}{(z+x)^2} \right]^{1/2} \int_{-1}^1 dz \text{Re} \left[ \frac{1}{(z-x)^2} \right]^{1/2} : \quad (57)$$

Finally, in the high- $T$  limit,  $T \gg \omega_c$ ; the imaginary part of  $(q;!)$  becomes independent of  $E_N$ ; because of thermal averaging,

$$\begin{aligned} \text{Im}(q;!) &\approx 2 \int_0^1 \frac{J_n^2(qR_c)}{T} \tanh \frac{E_n + !}{2T} \tanh \frac{E_n}{2T} J_{n-m}^2(qR_c) H\left(\frac{E_n - E_m + !}{2}\right) \\ &\approx 2 \int_0^1 \frac{J_k^2(qR_c)}{T} H\left(\frac{! - k\omega_c}{2}\right) : \end{aligned} \quad (58)$$

Since  $H(x > 1) = 0$ ; the imaginary part of  $(q;!)$  as a function of  $!$  at  $T \ll \omega_c$  consists of a series of peaks (broadened by  $\omega_c$ ) around multiples of the cyclotron frequency.

Importantly, the imaginary part of the polarization operator is suppressed at high frequencies,  $! \gg qv_F$ . This follows from Eq. (58), since  $J_n^2(qR_c)$  is exponentially small when  $n \gg qR_c$ . This is analogous to the zero- $B$  case, where

$$\text{Im}(q;!; B=0) = 2 \int_0^1 \frac{!}{qv_F} (qv_F - !)^2 \quad (59)$$

with  $\chi(x)$  the step function, and can be traced back to the fact that at high frequencies the magnetic field becomes almost irrelevant, so that the polarization operator approaches its zero- $B$  form.<sup>23</sup>

## V. DRAG RESISTIVITY

In a strong magnetic field,  $\omega_c \gg 1$ , the intralayer Hall resistivity  $\rho_{xy}$  dominates over the longitudinal resistivity  $\rho_{xx}$ . Therefore, the drag resistivity is given by

$$\rho_{xx}^D = \frac{\rho_{xy}^{(1)} \rho_{yy}^{(2)}}{\rho_{yx}^{(2)}} : \quad (60)$$

Using Eq. (5), we get the expression for the longitudinal component of the drag resistivity in a strong magnetic field,

$$\begin{aligned} \rho_{xx}^D &= \frac{B}{en_{e1}} \frac{B}{en_{e2}} \frac{1}{8} \int_{-1}^1 \frac{d!}{2T \sinh^2(!=2T)} \\ &\quad \frac{d^2 q}{(2)^2} \rho_{yx}^{(1)}(q;!;B) \rho_{yx}^{(2)}(q;!;B) J_{12}(q;!)^2 : \end{aligned} \quad (61)$$

The overall minus sign in Eq. (61) is due to the relation  $\rho_{xy} = -\rho_{yx}$ . It follows that for identical layers, the longitudinal ( $\parallel \hat{q}$ ) component  $\rho_{yy}$  of the triangle vertex gives rise to negative drag, since  $\rho_{yy}(B) = -\rho_{yy}(B)$ ; while the transverse ( $\perp \hat{q}$ ) component  $\rho_{yx}$  yields positive drag,  $\rho_{yx}(B) = \rho_{yx}(B)$ :

Since the upper limit of the momentum integration in (61) is effectively set by the inverse interlayer distance,  $a^{-1}$ , the behavior of the transresistivity will essentially depend on the relation between  $R_c$  and  $a$ . Below, we mainly concentrate on the ballistic regime

$$\omega_c = R_c a \gg N \omega_c ; \quad (62)$$

which we consider as most relevant experimentally. In Sec. V D we will briefly consider other situations and discuss the evolution of the transresistivity with decreasing interlayer distance, from the diffusive ( $R_c a \ll 1$ ) to the ultra-ballistic ( $R_c a \gg N \omega_c$ ) regime.

A . Ballistic regime: Low temperatures ( $T \ll T_D$ )

In the low-temperature limit, the expressions derived for the triangle vertex  $\chi(q; \omega)$  at  $\omega = 0$  are sufficient, because frequencies in Eq. (61) are restricted to  $\omega < T_D$ . Let us analyze which of the contributions to the triangle vertex dominates, depending on the relation between  $q$  and  $l=R_c$ .

In the diffusive range of momenta,  $qR_c \ll 1$ , the leading contribution to the triangle vertex is given by Eq. (31); its magnitude can be estimated as

$$\frac{k_F}{2qR_c} \quad (63)$$

In the ballistic regime,  $qR_c \gg 1$ ; we have three competing contributions (see Sec. III C),

$$^{(l=qR_c)} \frac{k_F}{2(qR_c)^2}; \quad (64)$$

$$^{(l=c)} \frac{k_F}{l_c q R_c} \quad q R_c \frac{1}{l_c} \quad ^{(l=qR_c)}; \quad (65)$$

$$^{(q=k_F)} \frac{1}{2R_c} \frac{(qR_c)^2}{N} \quad ^{(l=qR_c)} \frac{q}{k_F} \frac{1}{l_c} \quad ^{(l=c)}; \quad (66)$$

Comparing these expressions, we find that the first contribution,  $^{(l=qR_c)}$ , dominates for  $qR_c \ll l_c$ , the second one,  $^{(l=c)}$ , is dominant for  $l_c = qR_c \ll N = l_c$ , while the last contribution,  $^{(q=k_F)}$ , becomes the largest one for  $qR_c \gg N = l_c$ . This is valid provided that the Landau level index  $N$  is sufficiently large,  $N > (l_c)^2$ . We will assume below that this condition is fulfilled.

Splitting the momentum integral in Eq. (61) into three parts, corresponding to regions of different behavior of the triangle vertex and polarization operator, we present the transresistivity in the following form,

$$\rho_{xx}^D = \frac{e^2 B^2}{8\pi^3} \frac{k_F}{2n_e} \sum_{l=1}^Z \frac{k_F}{2n_e} \int d\omega \frac{\omega^2}{2T \sinh^2(\omega/2T)} I(\omega); \quad (67)$$

$$I(\omega) = I_I(\omega) + I_{II}(\omega) + I_{III}(\omega); \quad (68)$$

where the subscript  $l=1;2$  in  $(\dots)_l$  refers to the layer  $l$ , and the contributions  $I_I$ ,  $I_{II}$ , and  $I_{III}$  in (67) are determined by the momentum domains  $qR_c \ll l$ ,  $l \ll qR_c \ll l_c$ , and  $qR_c \gg l_c$ , respectively. The corresponding expressions are given in Appendix D. Estimating all three terms, we find [see Eq. (D 12)] that the leading contribution is given by the last term,

$$I(\omega) \approx I_{III}(\omega) = \frac{1}{2\pi^3 a^2 R_c^2} \ln \frac{R_c}{a l_c} \frac{16}{l_c^2} \left( \frac{E_N}{2} \right) \left[ \frac{1}{2} - \left( \frac{E_N}{2} \right)^2 \right] \frac{16}{l_c^2} \left( \frac{E_N}{2} \right) \left[ \frac{1}{2} - \left( \frac{E_N}{2} \right)^2 \right];$$

$$\frac{1}{a^2 R_c^2} \frac{1}{l_c^2} \ln \frac{R_c}{a l_c} \quad (69)$$

Therefore, for  $T \ll T_D$  we get for identical layers

$$\rho_{xx}^D = \frac{32}{3\pi^2 e^2} \frac{1}{(k_F a)^2 (l_0 R_c)^2} \frac{T}{l_c} \ln \frac{R_c}{a l_c} \frac{E_N^2}{2} \left( \frac{E_N}{2} \right)^2; \quad (70)$$

Thus at low temperature  $T \ll T_D$ , the drag resistivity scales with the magnetic field and temperature as

$$\rho_{xx}^D / T^2 B \ln(B/B_0); \quad (71)$$

where  $B_0 = (m c/e) (\frac{1}{l_c} a^2 l_0)^{1/3}$  sets the upper boundary for the considered ballistic regime on the magnetic field axis.

If  $R_c$  differs slightly between the two layers (i.e., the concentrations are slightly different) so that  $R_c = a l_c \pm 1$ , the above calculation fully applies, with the only change in Eq. (70)

$$\frac{E_N^2}{2} \left( \frac{E_N}{2} \right)^2 \left[ 1 - \frac{E_N}{2} \right] \frac{E_N}{2} \left( \frac{E_N}{2} \right)^2 \quad (72)$$

$$\frac{E_N}{2} \left( \frac{E_N}{2} \right)^2 \quad (73)$$

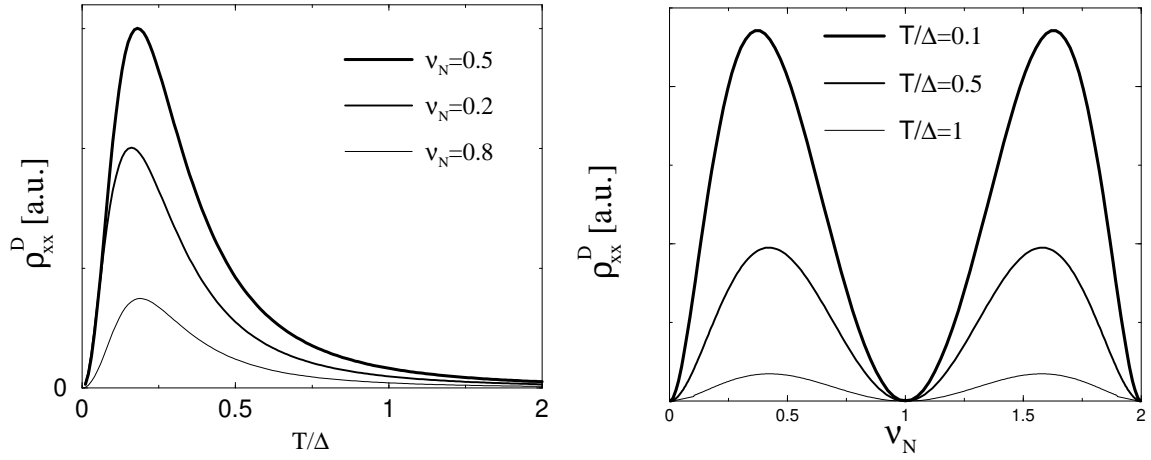


FIG. 6: Low-temperature drag for identical layers. Left panel: temperature dependences of the  $O(\omega_c)$ -term in  $\rho_{xx}^D(T)$  for different values of the filling factor of the highest LL,  $\nu_N = 0.5; 0.2; 0.8$  (from top to bottom). Right panel: dependence of the  $O(\omega_c)$ -term on the filling factor  $\nu_N$  for different values of temperature,  $T = 0.1; 0.5; 1$  (from top to bottom).

This yields an oscillatory sign of the drag. For identical layers the drag is positive, at variance with Ref. 14. This is because the leading term here originates from the component  $\hat{z}$  of the triangle vertex transverse to the wave vector  $q$  (i.e. directed along  $\hat{z} \times \hat{q}$ ). For a more detailed discussion of the sign of drag in different regimes, see Sec. V D.

If  $a < R_c < a + \omega_c$ , the calculation still applies, but the argument of the logarithm changes,

$$\ln \frac{R_c}{a + \omega_c} \rightarrow \ln \frac{R_c}{R_c - \omega_c} \quad (74)$$

#### B. Ballistic regime: Arbitrary $T = \tau v_F$

Having identified the leading contribution (coming from  $\omega_c$ -term) to drag for temperatures small compared to the LL width  $\omega_c$ , we generalize the obtained result to the case of larger  $T$  (and correspondingly  $\tau$ ). As discussed in Appendix D, the only difference in the momentum integral in the  $\omega_c$ -term is the replacement  $\omega_c \rightarrow T$  under the argument of logarithm. Using Eq. (39) and assuming that the difference in  $R_c$  between the two layers is not too large,  $R_c \approx a$ , we express the  $O(\omega_c)$ -contribution to the transresistivity as

$$\rho_{xx}^D(\omega_c) = \frac{4}{Z_1} \frac{1}{4e^2 (k_F a)^2 (\omega_c R_c)^2} \ln \frac{R_{cm} \max[\tau; T]}{a + \omega_c} \frac{d}{dT} \frac{F^*(\tau; T)_1 F^*(\tau; T)_2}{2T \sinh^2(\tau = 2T)} \quad (75)$$

where  $F^*(\tau; T)$  is a dimensionless function of  $\tau = \tau v_F$ ;  $(E_N) = \tau v_F$ ; and  $T = \tau v_F$ ;

$$F^*(\tau; T) = \frac{Z_1}{1} \frac{d}{dT} \frac{\tanh \frac{\tau + \omega_c}{2T}}{\tanh \frac{\tau - \omega_c}{2T}} \frac{1}{\frac{E_N}{1} \frac{(\tau + \omega_c - E_N)^2}{2}^{1/2}} \frac{1}{\frac{(\tau - \omega_c - E_N)^2}{2}^{1/2}} \quad (76)$$

For arbitrary  $T = \tau v_F$  this can only be calculated numerically. In Fig. 6 we present the results for the temperature dependence of the  $O(\omega_c)$ -contribution to drag as well as for its dependence on the filling factor  $\nu_N$  of the highest (partially filled,  $0 < \nu_N < 2$ ) LL. It is worth mentioning that when temperature is varied at fixed filling factor (as in typical experiments), the chemical potential is varying as well,  $\mu = \mu(\nu_N; T)$ ; which is taken into account in Fig. 6.

Consider the regime of temperatures large compared to the LL width,  $T \gg \omega_c$ . In this situation the LLs will be broadened by the temperature, so that typically  $E_N$  will be of order  $T$  and thus much larger than  $\omega_c$ . Expanding

the tanh-terms in (76) in  $\beta \ll T$  and  $E_N \ll T$ , we arrive at

$$\begin{aligned} D_{xx}^{(=1c)} &, \frac{4}{e^2} \frac{1}{(k_F a)^2 (\ell_0 R_c)^2} \ln \frac{R_c T}{a \ell_c} \\ & \sinh \frac{E_N}{2T} \cosh^3 \frac{E_N}{2T} \int_1^{\infty} \frac{\sinh \frac{E_N}{2T} \cosh^3 \frac{E_N}{2T}}{z^3} dz \\ & \frac{1}{T} \int_1^{\infty} \frac{d!}{z^2} [F(=2)]_1 [F(=2)]_2; \end{aligned} \quad (77)$$

where  $F(x)$  is a dimensionless function similar to Eq. (57). It also describes the overlap of two shifted Landau levels, but has an additional factor  $[(E_N) = ]^2$  arising from the particle(hole asymmetry due to LL quantization,

$$F(x) = \int_1^{\infty} dz z^{2n} \operatorname{Re} \int_1^{\infty} \frac{dz}{(z+x)^{2n}} \operatorname{Re} \int_1^{\infty} \frac{dz}{(z-x)^{2n}} \quad (78)$$

The contribution (77) scales as

$$D_{xx} / T^3 B^{7=2} \ln(T=B^2); \quad (79)$$

Since the above  $O(=1c)$ -term falls off quickly at  $T$ ; we should analyze the contributions of the other terms. Let us first calculate the "conventional" term  $O(q=k_F)$ ; substituting Eq. (45) in Eq. (61). Remarkably, the strong-B expression for the  $q=k_F$ -contribution to drag resistivity reduces to the standard zero-B form<sup>11,15,16</sup>,

$$\begin{aligned} D_{xx}^{(q=k_F)} &= \frac{1}{4 e^2 n_{e1} n_{e2}} \int_1^{\infty} \frac{d!}{2T \sinh^2(=2T)} \\ & \frac{d^2 q}{(q)^2} \operatorname{Im} (q;!)_1 \operatorname{Im} (q;!)_2 \mathcal{J}_{12}(q;!)^2; \end{aligned} \quad (80)$$

Here all the information about the magnetic field is encoded in  $(q;!)$ ; Eq. (49).

For  $T$ ; expanding the tanh-terms in  $\operatorname{Im} (q;!)$  just as before we find

$$\begin{aligned} D_{xx}^{(q=k_F)} &, \frac{3(3)}{2^4 e^2} \frac{1}{(k_F a)^4 (\ell_0 R_c)^2} \frac{\ell_c^2}{T} \\ & \cosh^2 \frac{E_N}{2T} \int_1^{\infty} \frac{\cosh^2 \frac{E_N}{2T}}{z^2} \int_1^{\infty} \frac{d!}{z^2} [H(=2)]_1 [H(=2)]_2; \end{aligned} \quad (81)$$

where  $\zeta(x)$  is the Riemann zeta-function [3]'<sup>1202</sup> and  $H(x)$  is defined in Eq. (57). This contribution scales as

$$D_{xx} / T^1 B^{7=2}; \quad (82)$$

The slower fall-off of the  $O(q=k_F)$ -contribution (81) as compared to (77) can be traced back to the different nature of the particle(hole asymmetry underlying these two contributions. Specifically, the  $O(=1c)$ -term (81) is governed by the particle(hole asymmetry due to the LL quantization. This is reflected by the factor  $E_N$  in (76) which after thermal averaging, translates into a factor in Eq. (77) which is asymmetric in  $E_N$ . On the other hand, the "conventional"  $q=k_F$  contribution is due to the curvature of zero-B spectrum and therefore is symmetric in  $E_N$  (and in  $E_N$  after thermal averaging). In both cases the fall-off of drag at  $T$  is due to the absence of electronic states outside the Landau band (for  $j = E_N, j > 0$ ). However, the thermal averaging of the odd function of  $E_N$  yields an additional factor  $=T$  for each  $=1c$ -triangle vertex, at variance with the case of an even function of  $E_N$  determining  $O(q=k_F)$ -contribution.

Finally, we evaluate the contribution of  $O(1=qR_c)$ -term. On the one hand, the thermal averaging suppresses each  $(1=qR_c)$  vertex by the factor  $(=T)^2$ , similarly to the  $O(=1c)$ -term. This is again because of the particle(hole asymmetry due to the LL quantization. On the other hand, the peculiarity of the finite-T screening gives rise to a factor  $(T=)^2$  in the momentum integral involving the  $O(1=qR_c)$ -term, see Appendix D. The remaining frequency integral yields the factor  $T=$ , since the allowed frequencies are restricted by  $|j| < 2 T$ . As a result, the contribution of this term to the drag resistivity is inversely proportional to temperature for  $T$ ; similarly to the conventional  $q=k_F$ -contribution. For simplicity we restrict ourselves to the case of identical layers, where we get

$$D_{xx}^{(1=qR_c)} , \frac{C^{(1=qR_c)}}{e^2} \frac{1}{(k_F a)^2 (\ell_0 R_c)^2 T} \sinh^2 \frac{E_N}{2T} \cosh^2 \frac{E_N}{2T}; \quad (83)$$

where  $c^{(1=qR_c)}$  is a constant of order unity,

$$c^{(1=qR_c)} = \frac{4}{\pi} \int_0^1 dx [P(x)]^2 W(x); \quad (84)$$

with the function  $W(x)$  defined in Eq. (D 20) and

$$P(x) = \int_0^1 dz z (z+x) \operatorname{Re} \left[ \frac{1}{(z+x)^2} \right]^{1=2} \operatorname{Re} \left[ \frac{1}{(z-x)^2} \right]^{1=2} \operatorname{O}_2; \quad (85)$$

This contribution scales as

$$\frac{D_{xx}}{T} / T^{-1} B^{5=2}; \quad (86)$$

We thus conclude that the  $O(1=qR_c)$ -contribution wins over the  $O(=1_c)$ -contribution for

$$T > \ln^{1=2} \frac{R_c}{a} \frac{1_c}{a}; \quad T:$$

Comparing (81) and (83), we have

$$\frac{O(q=k_F)}{D(1=qR_c)} \frac{1}{(k_F a)^2} (1_c)^2 \frac{R_c}{a} \frac{1_c}{N} \frac{1}{a}; \quad (87)$$

as follows from Eq. (62). Therefore the  $O(1=qR_c)$ -contribution dominates the drag resistivity in the intermediate range of temperature. This contribution oscillates with changing the filling factor of the two layers; however, it is negative for matching densities, unlike the  $O(=1_c)$ -contribution.

For higher temperatures,  $T > 1_c$ ; the terms related to the LL particle-hole asymmetry fall off rapidly due to the thermal averaging involving many LLs and thus the  $q=k_F$ -term (i.e. the "conventional" contribution to the drag resistivity) soon becomes dominant. The drag resistivity is then always positive, independently of the difference in filling factors of the two layers. It monotonously increases with increasing  $T$  and takes the form

$$\begin{aligned} \frac{D_{xx}}{T} &, \frac{8}{\pi^2} \frac{(3)}{e^2} \frac{1}{(k_F a)^4 (v_F R_c)^2} \frac{1_c}{E_F} \frac{T}{1_c} \int_0^1 \frac{d!}{2} [H(!=2)]_1 [H(!=2)]_2 \\ & \frac{1}{e^2 (k_F a)^2 (v_F a)^2} \frac{T}{E_F} \frac{1_c}{1_c} / T^2 B^{1=2}; \end{aligned} \quad (88)$$

This is almost the same result that is found in zero magnetic field<sup>11,15,16</sup>; the only difference is an extra factor  $1_c = v_F / B^{1=2}$ . The reason for the emergence of the zero-B result is physically very transparent. Characteristic frequencies  $1_c = T / 1_c$  set a characteristic time scale  $T^{-1}$ , which is much smaller than the time of the cyclotron revolution. At such times the electron motion is essentially unaffected by the magnetic field. The magnetic field enters, however, through the density of states inside the LL, which determines the characteristic magnitude of  $\operatorname{Im} \chi$ , and thus of  $\chi$ , see Eq. (45). The  $!$ -integration in (61) thus results in an effective averaging of  $1_c^2$ , yielding the factor  $1_c =$ . It is worth mentioning that, for the same reason, the longitudinal resistivity  $\rho_{xx}$  of a single layer is also enhanced by such a factor in the regime  $T > 1_c$  as compared to its zero-B value, see e.g. Ref. 24.

For still higher temperature,  $T > v_F = a$ ; the quadratic-in- $T$  dependence of the drag resistivity crosses over into the linear-in- $T$  drag. This occurs because of the suppression of the imaginary part of the polarization operator [determining the  $q=k_F$ -triangle, Eq. (45)] at  $! < v_F$ , see Eq. (59). As a result, the domain of  $!$ -integration is effectively restricted by  $! < v_F = a$  (since  $q < 1=a$ ), yielding the replacement  $T^2 / T v_F = a$  as compared to the case of  $! < T < v_F = a$ ,

$$\frac{D_{xx}}{T} / T B^{1=2};$$

Before closing this subsection, it is worth mentioning that in the above consideration we have neglected the contribution of magnetoplasmons to the drag (see Ref. 13 for details). While this contribution may become important for very high temperatures,  $T > 1_c$ ; it is negligibly small at relatively low  $T < 1_c$ ; which is the range of our main interest in the present paper.

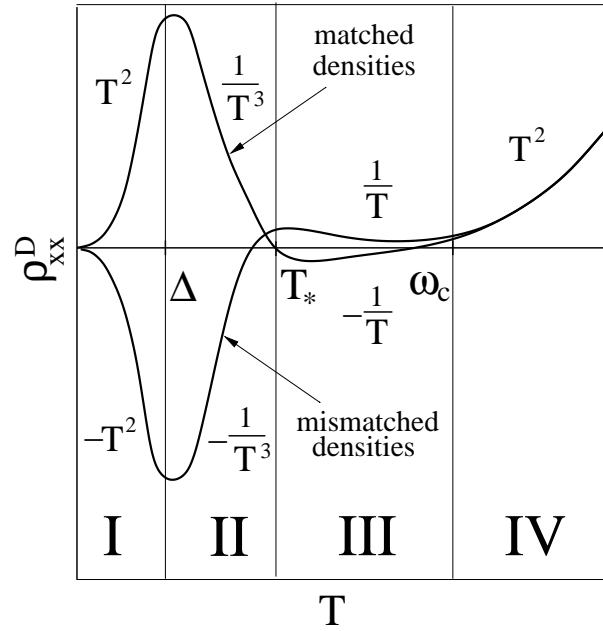


FIG. 7: Schematic temperature dependence of drag in the ballistic regime for matched and mismatched densities. In the latter case the mismatch is chosen such that the drag is negative at low  $T$  (see text). Scaling of  $\rho_{xx}^D$  with temperature in different regions is indicated: I { Eq. (71), II { Eq. (79), III { Eq. (86), and IV { Eq. (88).

#### C. Comparison with Experiment

In this subsection we compare the results for the drag in the ballistic regime obtained above with experimental findings. We have found a sequence of different regimes of the temperature behavior of  $\rho_{xx}^D$ , see Eqs. (71), (79), (86), (88). All these results are schematically summarized in Fig. 7. The upper curves there depicts  $\rho_{xx}^D(T)$  for equal densities, whereas the lower curve corresponds to a mismatch in densities chosen in such a way that the Fermi energy is located in the upper half of the Landau band in one layer, and in the lower half in the other layer. As has been already emphasized, the drag at low temperatures is positive for matched and negative for mismatched densities. This sign of the oscillatory drag can be traced back to the fact that the dominant contribution to the triangle vertex is given by  $\langle \sigma^{\perp} \rangle$ , which is transverse with respect to the momentum  $q$ .

We now compare these results with a most recent and detailed study by Muraki et al.<sup>10</sup> of the Coulomb drag in the regime of high Landau levels. A comparison of our Fig. 7 with Fig. 3 of Ref. 10 reveals a remarkable agreement between the experimental findings and our theoretical results. In both the theory and the experiment, (i)  $\rho_{xx}^D(T)$  shows a sharp peak at low temperatures; (ii) the sign of the drag in this temperature range oscillates as a function of the filling factor of one layer (at fixed filling factor of the other layer); (iii) the low- $T$  drag is positive for equal filling factors and negative when the Fermi energy in one layer is in the upper half and in the other layer in the lower half of the Landau band; (iv) the high- $T$  drag is always positive, independently of the difference in filling factors of two layers and increases monotonically with increasing  $T$ . Furthermore, it was observed by Muraki et al (see Fig. 2 of Ref. 10) that in the low-temperature regime of initial increase of  $\rho_{xx}^D$ , as well as in the high-temperature regime of "normal" drag, the drag resistivity can be described by an empirical scaling law,

$$\rho_{xx}^D / \frac{n}{B} \stackrel{2:7}{=} f(T=B) : \quad (89)$$

Our results for the low-temperature, (71), and high-temperature, (88), increase of  $\rho_{xx}^D$  are in a nice correspondence with this prediction, with  $f(x) \propto x^2$ .

The magnitude of the low-temperature peak in the drag resistivity that follows from our theory also agrees with the experiment. Specifically, estimating Eq. (70) at  $T = 0.25$  and  $[(E_N) = 1]^2 = 1=2$  by making use of typical experimental parameters,  $\mu_0 \approx 10^8 \text{ m}^{-1}$ ;  $a \approx 10^8 \text{ m}$ ,  $R_c \approx 10^7 \text{ m}$ , we find  $\rho_{xx}^D \approx 1$ ; in good agreement with the result of Ref. 10.

There is however a difference between our result (71) for the low-temperature scaling of drag and the interpretation of low- $T$  data in Ref. 10. Specifically, while we find  $T^2$  scaling in this regime, Muraki et al. fit the data to an exponential

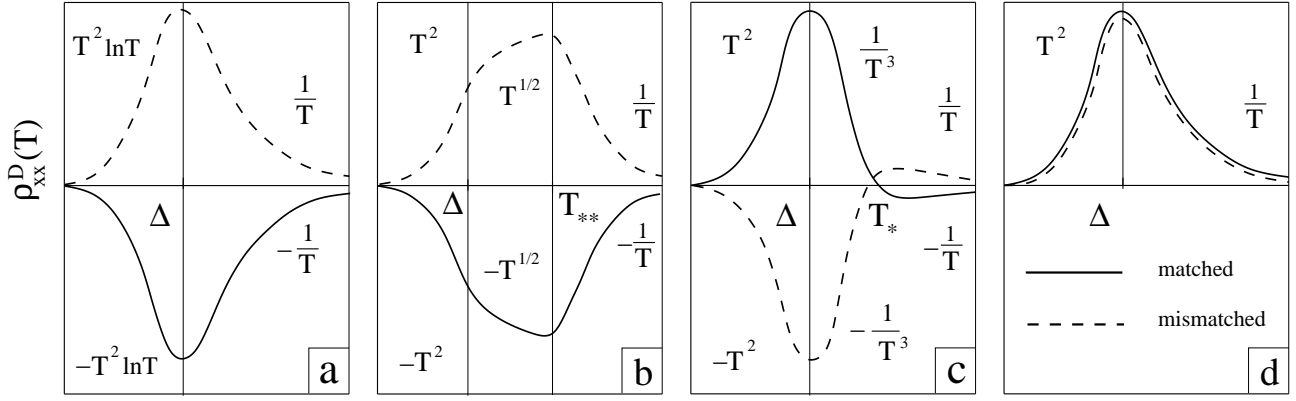


FIG. 8: Schematic temperature dependence of low-temperature drag in different regimes: a) diffusive,  $R_c = a \ll 1$ ; b) weakly ballistic,  $1 \ll R_c = a \ll \nu_c$ ; c) ballistic,  $\nu_c = R_c = a \ll N \ll \nu_c$ ; d) ultra-ballistic,  $N \ll \nu_c \ll R_c = a$ .

(activation-type) dependence, arguing that localized states are responsible for the low-temperature "anomalous peak" in  $\rho_{xx}^D(T)$ . We do not expect, however, that localization plays an important role in the regime of high Landau levels at realistic temperatures. Indeed, as is seen from Fig. 1 of Ref. 10, the resistivity for filling factors  $\nu > 10$  has a shape as predicted by SCBA, without developed Hall plateaus. Also, the fit of the low- $T$  behavior of  $\rho_{xx}^D$  to the activated over a single decade is not unambiguous; the same data could be quite well fitted to the  $T^2$  power law. In other words, we believe that our theory based on SCBA and not including quantum localization effects is sufficient to explain the most salient experimental observations of Ref. 10: the "anomalous" drag with oscillatory sign at low temperatures and the "normal" positive drag at high  $T$ .

D. Evolution of  $\rho_{xx}^D(T)$  with varying interlayer distance: From the diffusive to the ultra-ballistic limit.

As discussed in the beginning of Sec. V A, the form of the drag resistivity  $\rho_{xx}^D(T)$  depends on the value of the ratio  $R_c = a$ : In the above we have concentrated on the regime  $\nu_c = R_c = a \ll N \ll \nu_c$ ; which can be termed "ballistic" and which we believe to be most relevant to a typical experiment. In this subsection we briefly describe the results obtained for other regimes. Specifically, with increasing  $R_c = a$  we identify the following four regimes: i) diffusive,  $R_c = a \ll 1$ , ii) weakly ballistic,  $1 \ll R_c = a \ll \nu_c$ , iii) ballistic,  $\nu_c = R_c = a \ll N \ll \nu_c$ , and iv) ultra-ballistic,  $N \ll \nu_c \ll R_c = a$ . In all regimes, the temperature-dependence of the drag resistivity is non-monotonous: the absolute value of  $\rho_{xx}^D(T)$  shows a peak around  $T^*$  and increases again at  $T \gg \nu_c$ : However, the  $T$  and  $B$  dependences of  $\rho_{xx}^D$ , as well as the sign of the low-temperature peak (the high-temperature drag is always positive), are specific for each particular regime, as illustrated in Fig. 8 and summarized below.

Diffusive regime,  $R_c = a \ll 1$ . In the diffusive regime, the drag at not too high temperatures,  $T \ll \nu_c$ ; is governed by the diffusive rectification, Eqs. (31) and (32). As a result, the sign of the drag at  $T^*$  oscillates but is opposite to what we found above for the ballistic regime: the drag is negative for equal densities.<sup>14</sup> At the "slopes" of the peak,  $\rho_{xx}^D$  scales with  $T$  and  $B$  in the following way

$$\frac{\rho_{xx}^D}{\nu_c} \sim \begin{cases} T^2 \ln(TB^{3=2}); & T \ll \nu_c; \\ T^{-1} B^{3=2} \ln B; & T \gg \nu_c; \end{cases} \quad (90)$$

where the sign corresponds to the case of matching densities.

Weakly ballistic regime,  $1 \ll R_c = a \ll \nu_c$ . This regime is qualitatively similar to the diffusive regime. The peak at  $T^*$  is governed now by the  $O(1 = \nu_c R_c)$ -term in the triangle vertex, resulting in

$$\frac{\rho_{xx}^D}{\nu_c} \sim \begin{cases} T^2 B^{-5=4}; & T \ll \nu_c; \\ T^{1=2} B^{-1=2}; & T \sim \nu_c \quad (\nu_c = R_c); \\ T^{-1} B^{5=2}; & T \gg \nu_c \quad (\nu_c = R_c); \end{cases} \quad (91)$$

The sign of the peak oscillates just like in the diffusive regime.

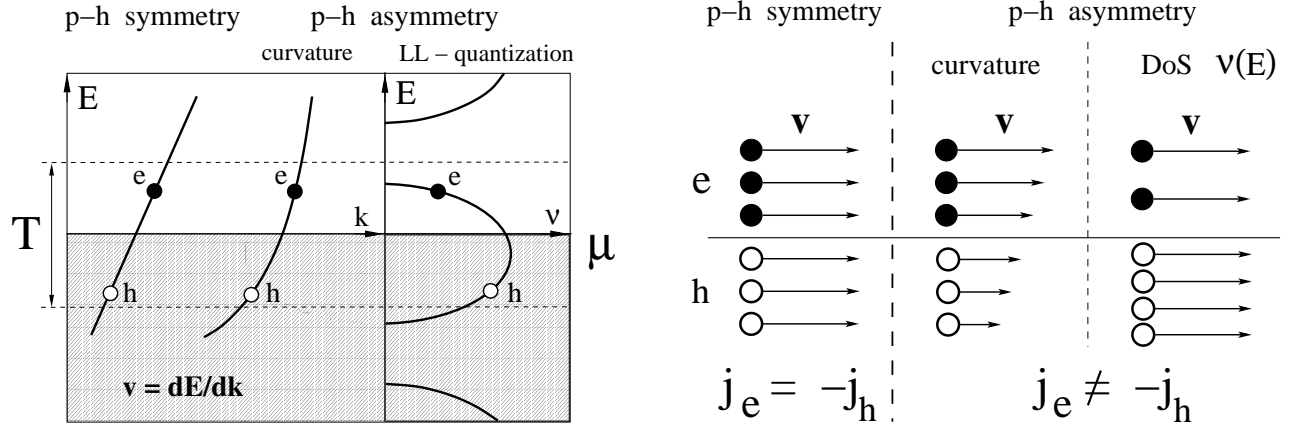


FIG. 9: Schematic illustration of different sources of particle-hole asymmetry: curvature of zero-B spectrum  $E(k)$  vs LL-quantization of the density of states (DoS)  $v(E)$ . In the particle-hole (p-h) symmetric case, the electronic and hole contributions to the current induced in the passive layer ( $j_e$  and  $j_h$ , respectively) compensate each other. When the p-h asymmetry is generated by a finite curvature, the velocities of electrons and holes (shown by arrows in the right panel) are different, which destroys the compensation. This is the "conventional" mechanism of the drag. When the DoS depends on energy (in the present case because of the LL-quantization), an "anomalous" drag arises due to the difference in numbers of occupied electronic and hole states.

Ballistic regime,  $\mu_c = R_c = a$ ,  $N = \mu_c$ . This is the regime we have studied in the main part of the paper. For the reader's convenience, we repeat the results here. The peak is governed by the  $O(\mu_c)$ -contribution, its sign oscillates and is positive for matching densities,

$$\frac{D_{xx}}{T} \sim \begin{cases} T^2 B \ln(B = B); & T > \mu_c; \\ T^3 B^{7=2} \ln(B = B); & T < \mu_c; \\ T^1 B^{5=2}; & T = \mu_c; \end{cases} \quad (92)$$

Ultra-ballistic regime,  $N = \mu_c$ ,  $R_c = a$ . The drag for all temperatures is determined by the conventional  $O(q=k_F)$ -contribution and is always positive,

$$\frac{D_{xx}}{T} \sim \begin{cases} T^2 B^2; & T > \mu_c; \\ T^1 B^{7=2}; & T < \mu_c; \end{cases} \quad (93)$$

At high temperature,  $T \gg \mu_c$ ; the drag is governed by the conventional contribution (and is therefore positive) in all the regimes. It is linear in  $T$  in the diffusive regime ( $D_{xx}/T B^{1=2}$ ). In all the ballistic regimes the drag resistivity scales as  $D_{xx}/T^2 B^{1=2}$  for  $\mu_c < T < v_F = a$  and  $D_{xx}/T B^{1=2}$  for  $T > v_F = a$ : (As mentioned in the end of Sec. V B, we do not consider the magnetoplasmon contribution<sup>13</sup> here.)

## VI. SUMMARY

In this paper, we have developed a systematic diagrammatic theory of the Coulomb drag in moderately strong magnetic fields, when the Landau bands are already separated but the Landau level index is still large. Using the self-consistent Born approximation, we performed a thorough analysis of all relevant contributions and, on this basis, analyzed the temperature dependence of the drag resistivity. Depending on the relation between the cyclotron radius  $R_c$  and the interlayer distance  $a$  we distinguish several regimes. We concentrated on the experimentally most relevant ballistic regime. In this case the theoretical analysis requires special care, in view of a cancellation between leading-order contributions to the triangle vertex. We also briefly considered the evolution of the drag resistivity in the whole range of  $R_c = a$ , from the diffusive to the ultra-ballistic regime.

We have shown that Coulomb drag in strong magnetic fields is an interplay of two contributions, as illustrated in Fig. 9. At high temperatures, the leading contribution is due to breaking of particle-hole symmetry by the curvature of the zero-B electron spectrum. This "normal" contribution to the drag is always positive and increases in a broad

temperature range as  $T^2$ . At low temperatures, we find that a second, "anomalous", contribution dominates, which arises from the breaking of particle-hole symmetry by the energy dependence of the density of states related to Landau quantization. This contribution is sharply peaked at a temperature  $T^*$  (where  $\Gamma$  is the Landau level width) and has an oscillatory sign depending on the density mismatch between the two layers. In particular, we find that in the ballistic regime the sign is positive for equal densities, in contrast to the negative sign in the diffusive regime found in Ref. 14.

Our results for the temperature dependence and sign of the drag resistivity  $\rho_{xx}^D(T)$  in the ballistic regime are illustrated in Fig. 7. These results are in good agreement with recent experimental findings<sup>10</sup>, and thus explain the remarkable features of Coulomb drag in high Landau levels observed experimentally.

Finally, we discuss some prospects for future research. First, our theory can be generalized to phonon drag, which is expected to dominate over Coulomb drag at larger separations between the layers. Second, it will be interesting to consider the magnetic field and temperature dependence of the drag around filling factor  $\nu = 1/2$ , where transport is due to composite fermions moving in a reduced magnetic field.<sup>25</sup> Third, one can study the effects of quantum localization, as well as criticality in the center of the Landau band,<sup>29</sup> which should become important in lower Landau levels or for very low temperatures. Finally, it should be possible to reproduce our results within the framework of a quantum kinetic equation [cf. Ref. 24]. This would also allow one to generalize the theory of magnetodrag to non-equilibrium setups (strong bias, microwave, etc.), as well as to other observables (e.g., the thermopower) related to particle-hole asymmetry.

#### Acknowledgments

We are grateful to K. von Klitzing, J.G.S. Lok, and K. Muraki for informing us on experimental results prior to publication and for interesting discussions. We further acknowledge valuable discussions with I.L. Aleiner, J. D. Pietel, A.V. Khaetskii, and A. Stern. FvO thanks the Weizmann Institute for hospitality and support through the Einstein Center and LSF while part of this work was performed. Financial support by the DFG-Schwerpunktprogramm "Quanten-Hall-Systeme" (IVG, ADM, and FvO), by SFB 290 and the "Junge Akademie" (FvO) is gratefully acknowledged.

#### APPENDIX A: ANALYTICAL CONTINUATION

In this Appendix we perform the analytical continuation of the Matsubara expressions for the drag conductivity and the triangle vertex. To calculate the Matsubara sum over  $n = 2nT$  in Eq. (3), the standard contour integration in the complex  $z$  plane is done,

$$T \sum_{n=2nT} f(in) = \frac{1}{4\pi i} \int_{C_b} dz f(z) \coth \frac{z}{2T}; \quad (\text{A } 1)$$

The integrand has branch cuts at  $\text{Im } z = 0$  and  $\text{Im } z = \omega_k$ ; where  $\omega_k$  represents the external frequency. The integration contour  $C_b$  thus contains three parts, see Fig. 10. Deforming the contour as shown in Fig. 10, we get four terms corresponding to four lines (above and below of both the branch cuts) forming the new contour,

$$\begin{aligned} \rho_{ij}^D(i\omega_k) = & \frac{e^2}{8\pi k S} \sum_q \int_0^1 dz \coth \frac{z}{2T} \\ & \times \left[ \begin{aligned} & \frac{1}{i} \binom{(1)}{q; i + i\omega_k; i + i0} \binom{(2)}{j} \binom{(2)}{q; i + i0; i + i\omega_k} U(q; i + i\omega_k) U(q; i + i0) \\ & \frac{1}{i} \binom{(1)}{q; i + i\omega_k; i0} \binom{(2)}{j} \binom{(2)}{q; i0; i + i\omega_k} U(q; i + i\omega_k) U(q; i0) \\ & + \frac{1}{i} \binom{(1)}{q; i + i0; i - i\omega_k} \binom{(2)}{j} \binom{(2)}{q; i - i\omega_k; i + i0} U(q; i + i0) U(q; i - i\omega_k) \\ & \frac{1}{i} \binom{(1)}{q; i0; i - i\omega_k} \binom{(2)}{j} \binom{(2)}{q; i - i\omega_k; i0} U(q; i0) U(q; i - i\omega_k) \end{aligned} \right]; \quad (\text{A } 2) \end{aligned}$$

In the third and fourth terms we have used  $\coth(z + i\omega_k/2T) = \coth z$ . The contributions of points  $z = 0$  and  $z = i\omega_k$  cancel the integral over the small circles around these points, so that the integrals above should be understood in the principal value sense.

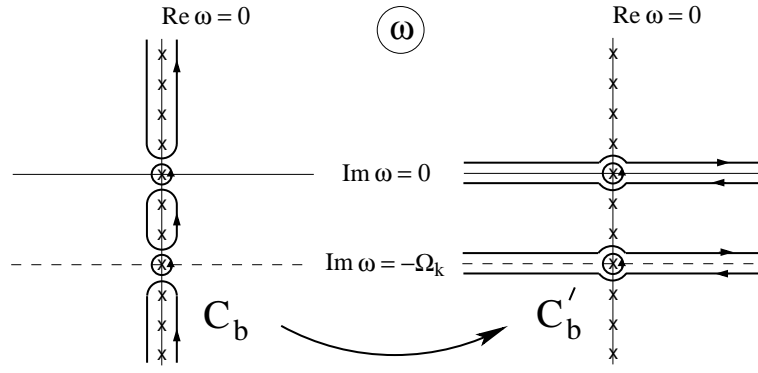


FIG. 10: Contours for the  $\omega$ -integration.

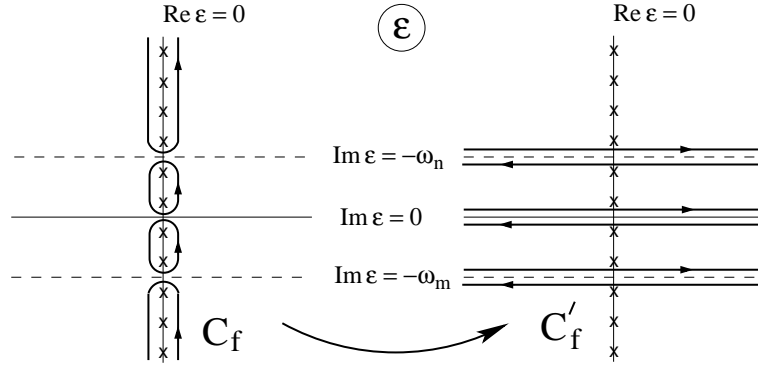


FIG. 11: Contours for the  $\epsilon$ -integration.

We now perform the analytical continuation  $i_k \rightarrow i_k + i0$  and take the limit  $i0 \rightarrow 0$ . As shown in Ref. 15, the first and the last terms coming from outer sides of branch cuts vanish in the limit  $i0 \rightarrow 0$ . This yields

$$D_{ij} = \frac{e^2}{8S} \sum_q \int_1^{Z_1} d! \coth \frac{!}{2T} \frac{\partial}{\partial !} h_i^{(1)}(q; ! + i0; ! - i0) h_j^{(2)}(q; ! - i0; ! + i0) U(q; ! + i0) U(q; ! - i0); \quad (A 3)$$

Using

$$\frac{\partial}{\partial !} \coth \frac{!}{2T} = \frac{1}{2T \sinh^2 (!/2T)}; \quad (A 4)$$

we arrive at Eq. (5).

The next step is the analytical continuation of the triangle vertex. The summation over the fermionic Matsubara energies  $i_k = 2\pi(k + 1/2)T$  in Eq. (4) is performed using the integral

$$\sum_k f(i_k) = \frac{1}{4\pi} \int_{C_f}^Z d f(z) \tanh \frac{z}{2T}; \quad (A 5)$$

along the contour  $C_f$  shown in Fig. 11. Since the triangle vertex depends on two frequencies  $i_m$  and  $i_n$ , the integrand now has three branch cuts in the complex plane of  $z$ , namely at  $\text{Im } z = 0$ ;  $\text{Im } z = -i\omega_n$ ; and  $\text{Im } z = -i\omega_m$ . Similarly to  $C_b$ , the contour  $C_f$  can be deformed into a set of six lines going on both sides of each of the branch cuts (see Fig. 11), yielding

$$(q; i_m, i_n) = \int_1^{Z_1} \frac{d}{4\pi} \tanh \frac{z}{2T}$$

$$\begin{aligned}
& \text{tr } v \left[ \mathbb{G}^+ (\mathbf{r}) - G (\mathbf{r}) \right] e^{iqx} G (\mathbf{r} - i\mathbf{l}_n) e^{-iqx} G (\mathbf{r} + i\mathbf{l}_m - i\mathbf{l}_n) \\
& v G (\mathbf{r} + i\mathbf{l}_n) e^{iqx} \left[ \mathbb{G}^+ (\mathbf{r}) - G (\mathbf{r}) \right] e^{-iqx} G (\mathbf{r} + i\mathbf{l}_m) \\
& + v G (\mathbf{r} - i\mathbf{l}_m + i\mathbf{l}_n) e^{iqx} G (\mathbf{r} - i\mathbf{l}_m) e^{-iqx} \left[ \mathbb{G}^+ (\mathbf{r}) - G (\mathbf{r}) \right] \\
& + (i\mathbf{l}_n \cdot \mathbf{l}_m; q; \mathbf{r}):
\end{aligned} \tag{A 6}$$

In this formula  $G (\mathbf{r}) = G (\mathbf{r} - i0)$  and we have used  $\tanh (z - i\pi/2T) = \tanh (z - i\pi/2T) = \tanh z$ . The equation (A 6) is valid irrespective of the relation between  $\mathbf{l}_m$ ;  $\mathbf{l}_n$ ; and 0. Performing the analytical continuation to real frequencies  $i\mathbf{l}_m \cdot \mathbf{l}_1 + i0$  and  $i\mathbf{l}_n \cdot \mathbf{l}_2 - i0$  (and shifting the integration variables  $\mathbf{l} = \mathbf{l} + \frac{1}{2}$  and  $\mathbf{l} = \mathbf{l} + \frac{1}{2}$  in the first and third terms, respectively) we obtain

$$\begin{aligned}
(q; \mathbf{l}_1 + i0; \mathbf{l}_2 - i0) &= \int_{-1}^1 \frac{d}{4i} \\
& \text{tr } \tanh \frac{\mathbf{l}_2}{2T} v \left[ \mathbb{G}^+ (\mathbf{r} + \mathbf{l}_2) - G (\mathbf{r} + \mathbf{l}_2) \right] e^{iqx} G^+ (\mathbf{r}) e^{-iqx} G^+ (\mathbf{r} + \mathbf{l}_1) \\
& \tanh \frac{\mathbf{l}_1}{2T} v G (\mathbf{r} + \mathbf{l}_2) e^{iqx} \left[ \mathbb{G}^+ (\mathbf{r}) - G (\mathbf{r}) \right] e^{-iqx} G^+ (\mathbf{r} + \mathbf{l}_1) \\
& + \tanh \frac{\mathbf{l}_1}{2T} v G (\mathbf{r} + \mathbf{l}_2) e^{iqx} G (\mathbf{r}) e^{-iqx} \left[ \mathbb{G}^+ (\mathbf{r} + \mathbf{l}_1) - G (\mathbf{r} + \mathbf{l}_1) \right] \\
& + (i; q; \mathbf{l}; \mathbf{r}):
\end{aligned} \tag{A 7}$$

Setting  $\mathbf{l}_1 = \mathbf{l}_2$  and collecting the contributions containing only retarded (from the first term) and only advanced (from the third term) Green functions, we arrive [up to a redefinition of zero of fermionic energies, which are counted from the chemical potential in Eq. (A 7)] at Eq. (7) for <sup>(a)</sup>. The remaining terms constitute the expression (8) for <sup>(b)</sup>.

## APPENDIX B: VERTEX CORRECTIONS IN SCBA

In this appendix, we review vertex corrections in SCBA. We start by noting that in real space, the impurity-averaged electron Green function in SCBA can be written as

$$G (\mathbf{r}; \mathbf{r}^0; E) = e^{i\mathbf{r} \cdot (\mathbf{r}; \mathbf{r}^0)} \sum_n C_n (\mathbf{r} - \mathbf{r}^0) G_n (E) \tag{B 1}$$

with

$$C_n (\mathbf{r}; \mathbf{r}^0) = \frac{1}{2} e^{-i\mathbf{r} \cdot \mathbf{r}^0} L_n \left( \frac{\mathbf{r} - \mathbf{r}^0}{2} \right) : \tag{B 2}$$

The gauge-dependent phase  $\mathbf{r} \cdot (\mathbf{r}; \mathbf{r}^0)$  satisfies  $\mathbf{r} \cdot (\mathbf{r}; \mathbf{r}^0) = \mathbf{r} \cdot (\mathbf{r}^0; \mathbf{r})$ . This can be used to express the vertex correction in real space as (cf. Fig. 12)

$$(q; \mathbf{l}; \mathbf{r}) = e^{iqx} + \frac{1}{2} \int_{-1}^1 dr^0 (q; \mathbf{l}; \mathbf{r}^0) G (\mathbf{r}; \mathbf{r}^0; E + i) G (\mathbf{r}^0; \mathbf{r}; E) : \tag{B 3}$$

For well-separated Landau levels, the valence LL with LL index  $N$  gives the dominant contribution so that

$$(q; \mathbf{l}; \mathbf{r}) = e^{iqx} + \frac{1}{2} G_N (E + i) G_N (E) \int_{-1}^1 dr^0 C_N (\mathbf{r} - \mathbf{r}^0) C_N (\mathbf{r}^0 - \mathbf{r}) (q; \mathbf{l}; \mathbf{r}^0) : \tag{B 4}$$

Thus, we find that

$$(q; \mathbf{l}; \mathbf{r}) = (q; \mathbf{l}; \mathbf{r}^0) e^{iqx} \tag{B 5}$$

with

$$(q; \mathbf{l}; \mathbf{r}^0) = 1 + \frac{(2 - \mathbf{v})^2}{4} (q; \mathbf{l}; \mathbf{r}^0) G_N (E + i) G_N (E) \int_{-1}^1 dr^0 C_N (\mathbf{r} - \mathbf{r}^0) C_N (\mathbf{r}^0 - \mathbf{r}) e^{iq(\mathbf{r} - \mathbf{r}^0)} : \tag{B 6}$$

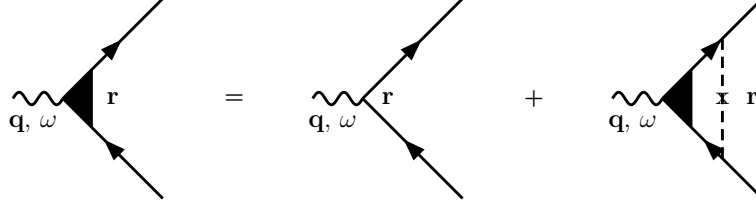


FIG. 12: Diagrams for the (scalar) vertex corrections in real space.

Here we used the identity  $\int_{\mathbb{Z}} dr^0 C_N(r^0) C_N(r^0 - r) e^{iq(r^0 - r^0)} = \frac{1}{2} \int_{\mathbb{Z}} dr^0 e^{iq^2 r^0} [C_N(q^2 r^0 = 2)]^2$ . The integral is equal to

$$\int_{\mathbb{Z}} dr^0 C_N(r^0) C_N(r^0 - r) e^{iq(r^0 - r^0)} = \frac{1}{2} \int_{\mathbb{Z}} dr^0 e^{iq^2 r^0} [C_N(q^2 r^0 = 2)]^2$$

$$= \frac{1}{2} \int_{\mathbb{Z}} dr^0 J_0^2(qR_c); \quad (\text{B } 7)$$

where the second equality holds in the limit of high Landau levels. Neglecting the frequency-dependence and using the identities

$$G_N^+ G_N = \frac{4}{2} \quad (\text{B } 8)$$

$$G_N^+ G_N^+ = \frac{1}{\binom{N}{N}^2}; \quad (\text{B } 9)$$

we can solve for  $\Gamma$ , and obtain Eqs. (18) and (19) for the vertex corrections. Finally, for finite  $N$  we get

$$\Gamma(q;!) = \frac{1}{1 - \binom{N}{N} J_0^2(qR_c) G_N^+ (E +!) G_N^+ (E)}; \quad (\text{B } 10)$$

which is used in Eq. (28).

### APPENDIX C: CORRECTIONS OF ORDER $\propto c$

In this appendix, we consider the contributions to the triangle vertex to order  $\propto c$  in more detail. To this order, vertex corrections of the scalar vertices can be neglected.

We first consider the case (i) in which both Green functions adjacent to the current vertex are evaluated in Landau levels other than  $N$ . As mentioned in Sec. III C 2, the Green function connecting the scalar vertices should be evaluated in the  $N$ th LL up to corrections of order  $(\propto c)^2$ . Using the semiclassical expression (23) for the matrix elements, we then find for the corresponding correction to  $\Gamma$  the expression

$$\begin{aligned} \Gamma^{(b)}(q;!) &= \frac{!}{i} \frac{1}{2} \int_{\mathbb{Z}} dr^0 \frac{P}{2} (G_N^+ G_N) \sum_{n \notin N, N+1} X \frac{2i}{0} \frac{1}{(N-n)!_c} \frac{1}{(N-n+1)!_c} i J_{N-n+1}(qR_c) J_{N-n}(qR_c) \\ &= \frac{!}{2} \frac{1}{2} \int_{\mathbb{Z}} dr^0 \frac{P}{2} (G_N^+ G_N) \sum_{k=1}^X \frac{1}{k(k+1)} \frac{2i}{0} [J_k(qR_c) J_{k+1}(qR_c) + J_{-k}(qR_c) J_{-(k+1)}(qR_c)]; \quad (\text{C } 1) \end{aligned}$$

Using that  $J_{-k}(z) = (-1)^k J_k(z)$ , we find that the expression in square brackets vanishes so that  $\Gamma^{(b)}(q;!) = 0$ .

The corresponding contribution to  $\Gamma$  takes the form

$$\begin{aligned} \Gamma^{(a)}(q;!) &= \frac{!}{2} \frac{1}{2} \int_{\mathbb{Z}} dr^0 \frac{P}{2} \frac{\partial}{\partial q_{n \neq m}} X J_{n-m}^2(qR_c) G_m^+ G_n^+ \\ &= \frac{2!}{2} \frac{1}{2} \int_{\mathbb{Z}} dr^0 \frac{P}{2} \frac{\partial}{\partial q_{k=1}} X J_k^2(qR_c) (G_N^+ G_{N-k}^+ + G_N^+ G_{N+k}^+); \quad (\text{C } 2) \end{aligned}$$

The prime on the sum indicates that only those terms should be kept, in which one of the two Green functions is evaluated in a LL different from  $N$ . In leading order,

$$G_{N-k}^+ = G_{N+k}^+ = \frac{1}{k!_c};$$

and hence also the contribution (C 2) to the triangle vertex vanishes.

Next, we turn to the contribution (ii) in which the diagrams in Fig. 4 are evaluated to next-to-leading order in  $\omega/c$  while neglecting the vertex corrections on the scalar vertices. Such contributions can arise in particular from the self energy entering  $G_{N-1}$ . We first consider the corresponding contribution to  $\chi_x^{(b)}$ . (For the purpose of this appendix, we choose  $q \times \hat{x}$ .) According to the diagrams in Fig. 4, we have for the contribution (ii)

$$\chi_x^{(b)} = \frac{i!}{2} \frac{1}{v} \frac{P}{\gamma_m} \frac{N}{2} J_0(qR_c) J_1(qR_c) 2 \text{Im} (G_{N-1} G_{N+1}) [G_N^+]^2; \quad (\text{C } 3)$$

Here, we have already used that to the order under consideration,

$$(G_{N-1} G_{N+1}) G_N^+ G_N + (G_{N-1}^+ G_{N+1}^+) G_N^+ G_N \neq 0; \quad (\text{C } 4)$$

To our order, we then find

$$\chi_x^{(b)} = \frac{i!}{2} \frac{2N}{v} J_0(qR_c) J_1(qR_c) \text{Im} [G_N^+]^2; \quad (\text{C } 5)$$

Comparing with Eq. (25), we find even to order  $\omega/c$  that this contribution is cancelled exactly by  $\chi_x^{(a)}$ . Thus, there is also no contribution of type (ii) to  $\chi_x$  and  $\chi_x$  vanishes to order  $\omega/c$ .

Finally, we consider the contribution of type (ii) to  $\chi_y$ . Since this is a transverse contribution, we need to consider only  $\chi_y^{(b)}$ . In this case, the diagrams in Fig. 4 translate into the expression

$$\chi_y^{(b)} = \frac{i!}{2} \frac{1}{v} \frac{P}{\gamma_m} \frac{N}{2} i J_0(qR_c) J_1(qR_c) (G_{N-1}^+ G_N + G_N G_{N+1}^+) 2i \text{Im} (G_{N-1} + G_{N+1}) G_N^+; \quad (\text{C } 6)$$

Noting that the leading order cancels from the combination,  $G_{N-1} + G_{N+1}$ , we can simply evaluate Eq. (C 6) for  $\chi_y$  to leading nonvanishing order. This yields Eq. (38) for  $\chi_y^{(\omega/c)}$  in the main text.

#### APPENDIX D : CONTRIBUTIONS TO DRAG FROM DIFFERENT MOMENTUM REGIONS

We write down explicitly the momentum integrals determining the function  $I(\omega)$  in Eq. (67). The first integral, corresponding to the dispersive range of momenta  $qR_c \ll 1$ ;

$$I_I(\omega) = \int_0^{Z_{1=R_c}} \frac{dq}{2} \frac{q}{\sinh qa} \frac{q^2}{2} \frac{4qR_c \frac{(E_N) D(\omega) q^2}{D(\omega) q^2 \mathcal{J}^2 + \omega^2}}{2} \frac{4qR_c \frac{(E_N) D(\omega) q^2}{D(\omega) q^2 \mathcal{J}^2 + \omega^2}}{2} \frac{2}{(E_N)^2} \frac{2}{2!c} \frac{D(\omega) q^2 \mathcal{J}^2 + \omega^2}{D(\omega) q^2 \mathcal{J}^2}; \quad (\text{D } 1)$$

is dominated by the contribution of the "dispersive rectification", Eq. (31), while the screening is determined by Eq. (34). The second integral

$$I_{II}(\omega) = I_{II1}(\omega) + I_{II2}(\omega); \quad (\text{D } 2)$$

includes the contribution of  $(1=qR_c)$  [denoted by  $I_{II1}(\omega)$ ] and  $(\omega/c)$  [denoted by  $I_{II2}(\omega)$ ], Eqs. (36) and (38), respectively, while the screening in  $I_{II}$  is determined by Nth LL, Eq. (51).

$$I_{II1}(\omega) = \int_{1=R_c}^{Z_{1=c=R_c}} \frac{dq}{2} \frac{q}{\sinh qa} \frac{q^2}{2} J_1(qR_c) J_0^3(qR_c) \frac{64}{4} (E_N)^2 \frac{64}{4} (E_N)^2 \frac{8!c}{3} J_0^2(qR_c) \frac{(E_N)^2}{2} \frac{8!c}{3} J_0^2(qR_c) \frac{(E_N)^2}{2}; \quad (\text{D } 3)$$

$$I_{II2}(\omega) = \int_{1=R_c}^{Z_{1=c=R_c}} \frac{dq}{2} \frac{q}{\sinh qa} \frac{q^2}{2} f J_1(qR_c) J_0(qR_c) g_1 - f J_1(qR_c) J_0(qR_c) g_2$$

$$\left( \frac{16}{\epsilon_c^2} (E_N)^2 - (E_N)^2 \right) \frac{16}{\epsilon_c^2} (E_N)^2 - (E_N)^2 \left( 1 + \frac{8\epsilon_c}{3} J_0^2(qR_c) \right) \frac{16}{\epsilon_c^2} (E_N)^2 - (E_N)^2 \left( 1 + \frac{8\epsilon_c}{3} J_0^2(qR_c) \right) \frac{16}{\epsilon_c^2} (E_N)^2 - (E_N)^2 : \quad (D 4)$$

The integration domain in the third integral,  $I_{III}(!)$ ; corresponds to the range where the screening acquires its static zero-B form, Eq. (53), while the triangle vertex is dominated by  $(\epsilon_c)$ , Eq. (38),

$$I_{III}(!) = \int_{\epsilon_c = R_c}^Z \frac{dq q}{2} \frac{q}{\sinh qa} f_{J_1}(qR_c) J_0(qR_c) g_1 f_{J_1}(qR_c) J_0(qR_c) g_2 \frac{16}{\epsilon_c^2} (E_N)^2 - (E_N)^2 \frac{16}{\epsilon_c^2} (E_N)^2 - (E_N)^2 \quad (D 5)$$

Let us analyze the first term in  $I_{II}$ , Eq. (D 3). Consider identical layers. The screening is nontrivial and almost vanishes in the vicinity of zeroes  $Q_n$  of  $J_0^2(qR_c)$ . The structure of the integral is

$$I_{II 1} / \int_{\epsilon_c = R_c}^Z \frac{dq q}{1 + A J_0^2(qR_c)} \frac{J_1^2(qR_c) J_0^6(qR_c)}{[1 + A J_0^2(qR_c)]^4}; \quad (D 6)$$

where  $A = \epsilon_c$ . We see that the integral is dominated by the momenta close to  $Q_n$ , each peak contributing  $R_c^2 Q_n^{1=2} A^{-7=2}$ , so that the total result

$$I_{II 1} / \frac{1}{R_c^2} \sum_n Q_n^{1=2} \frac{\epsilon_c^{-7=2}}{R_c^2 \epsilon_c} \int_{\epsilon_c = R_c}^Z dQ Q^{1=2} \frac{1}{R_c^2 \epsilon_c} ; \quad (D 7)$$

is determined by the upper limit where  $A J_1^2(qR_c) = 1$ :

Similarly, we estimate the second term in  $I_{II}$ , Eq. (D 4),

$$I_{II 2} / \int_{\epsilon_c = R_c}^Z \frac{dq q}{1 + A J_0^2(qR_c)} \frac{J_1^2(qR_c) J_0^2(qR_c)}{[1 + A J_0^2(qR_c)]^4} \frac{1}{R_c^2 \epsilon_c} \int_{\epsilon_c = R_c}^{9=2 Z} dQ Q^{3=2} \frac{1}{R_c^2 \epsilon_c} ; \quad (D 8)$$

yielding the result of the same order as for Eq. (D 3), since both integrals are dominated by the upper limit. We note that for this reason the same estimate can be obtained by replacing  $J_0^2(qR_c); J_1^2(qR_c)$  by  $(qR_c)^{-1}$ : The two terms  $I_{II 1}$  and  $I_{II 2}$  give contributions of the opposite signs to the drag resistivity, since  $O(1=qR_c) \propto j_j(B) = j_j(B)$ , while  $O(\epsilon_c) \propto j_j(B) = j_j(B)$ .

Estimating other terms, we obtain

$$I_I = \frac{1}{a^2 R_c^2 \epsilon_c} \int_{Q_{min}}^Z \frac{dQ}{Q} = \frac{1}{a^2 R_c^2 \epsilon_c} \ln Q_{min}; \quad (D 9)$$

$$I_{II} = \frac{1}{a^2 R_c^2 \epsilon_c} \int_{\epsilon_c = R_c}^Z dQ Q^{1=2} \frac{1}{a^2 R_c^2 \epsilon_c} ; \quad (D 10)$$

$$I_{III} = \frac{1}{a^2 R_c^2 \epsilon_c} \int_{\epsilon_c = R_c}^Z \frac{dQ}{Q} = \frac{1}{a^2 R_c^2 \epsilon_c} \ln \frac{R_c}{a \epsilon_c} ; \quad (D 11)$$

where in the dissipative term  $I_I$  the momentum integration is restricted from below by  $Q_{min} = R_c (\epsilon_c = aD)^{1=2}$   $R_c (T = aD)^{1=2}$ : This infrared cut-off is necessary, since the momentum integral diverges logarithmically at small  $q$  in the dissipative regime, when Eq. (48) and Eq. (34) are used for the interlayer interaction. The divergence is naturally cured when the general formula (47) is employed together with Eq. (34).

Thus we conclude that at low temperatures  $T$  the total integral is dominated by the contribution of high momenta,  $I_{III}$ ;

$$I_I + I_{II} + I_{III} \approx I_{III} = \frac{1}{2^3 a^2 R_c^2 \epsilon_c} \ln \frac{R_c}{a \epsilon_c} \frac{16}{\epsilon_c^2} (E_N)^2 - (E_N)^2 \frac{16}{\epsilon_c^2} (E_N)^2 - (E_N)^2 ; \quad (D 12)$$

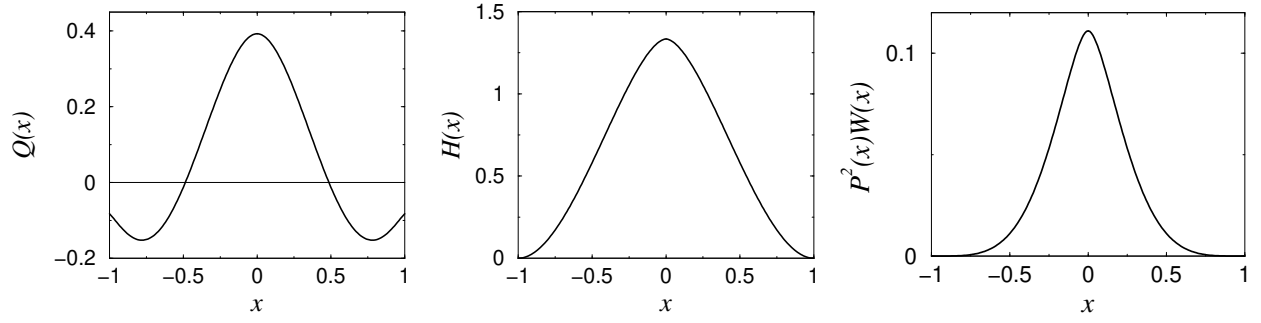


FIG. 13: Functions  $Q(x)$  { Eq. (55), and  $H(x)$  { Eq. (57), and the product  $P^2(x)W(x)$  { Eqs. (85) and (D 20), determining the frequency dependence of the \textit{inelastic kernel}  $I(\omega)$  { Eq. (D 15).

resulting in Eq. (70).

In the case of higher temperatures,  $T \gg \omega_c$ ; the main difference is related to the fact that the contribution of a single LL to the polarization operator is thermally smeared, yielding an extra factor  $\omega_c/T$  as compared to the second term of Eq. (51), as follows from Eq. (54). This changes the upper (lower) limit of integration in  $I_{II}$  ( $I_{III}$ ) where  $\omega_c$  should be replaced by  $T$ . Furthermore, in  $I_{II}$  one should replace  $\omega_c =$  by  $\omega_c = T$  in the factor related to the screening, which is equivalent to multiplying  $A$  by  $\omega_c/T$  in Eqs. (D 6) and (D 8). This yields

$$I_{II} = \frac{1}{a^2 R_c^2} \frac{T}{\omega_c^2}; \quad (D 13)$$

$$I_{III} = \frac{1}{a^2 R_c^2} \frac{1}{\omega_c^2} \ln \frac{R_c T}{a \omega_c}; \quad (D 14)$$

We see that for  $\omega_c < T < \omega_c$  the contribution of the  $(\omega = qR_c)$ -term to the momentum integral increases faster than that of  $(\omega = \omega_c)$ -term. To evaluate this contribution more accurately, we consider the corresponding momentum integral in the whole range of  $q$  and include the imaginary part of  $\epsilon(q; \omega)$  into the screening (for simplicity we consider identical layers),

$$I(\omega) = \frac{16}{T^2} P \frac{\omega^2}{2} \frac{\sinh^2 \frac{E_N}{2T} \cosh^6 \frac{E_N}{2T}}{\cosh^6 \frac{E_N}{2T}} I^{(\omega = qR_c)}; \quad (D 15)$$

$$I^{(\omega = qR_c)} = \int_{1=R_c}^{\omega_c} \frac{dq}{2} \frac{q^2}{\sinh qa} \frac{q J_1^2(qR_c) J_0^6(qR_c)}{f [1 + A J_0^2(qR_c)]^2 + [B J_0^2(qR_c)]^2 g^2}; \quad (D 16)$$

where  $P(x)$  is defined in Eq. (85) and

$$A = \frac{2\omega_c}{T} Q(\omega_c = 2) \cosh^2 \frac{E_N}{2T}; \quad (D 17)$$

$$B = \frac{2\omega_c}{T} H(\omega_c = 2) \cosh^2 \frac{E_N}{2T}; \quad (D 18)$$

according to Eqs. (54) and (56). The functions  $Q(x)$ ; and  $H(x)$  are presented in Fig. 13.

From the above estimates we know that the momentum integral is determined by  $q \approx \omega_c = TR_c$   $1=R_c$ : This holds provided  $A; B \approx \omega_c = T$   $1$ ; i.e. for  $\cosh(E_N/2T) \approx (\omega_c = T)^{1/2}$ : On the other hand,  $\omega_c = TR_c$   $1=a$  in the ballistic regime. In this case, we can set  $q^2 = \sinh^2 qa = 1/a^2$  in Eq. (D 16) and set the lower integration limit to  $q = 0$ . Separating the fast and slow variables in Eq. (D 16), we get  $[J_1(z_n) = 0; z_n' = n + 1/2]$

$$\begin{aligned} I^{(\omega = qR_c)} &= \frac{1}{2 a^2 R_c^2} \int_{z=0}^{\omega_c} \frac{2}{z_n} \int_0^{\omega_c} \frac{d}{f [1 + (2A = z_n) \cos^2] ^2 + [(2B = z_n) \cos^2] ^2 g^2} \\ &= \frac{2}{3 a^2 R_c^2} \int_0^{\omega_c} \frac{d \sin^2 \cos^2}{f [z + A]^2 + B^2 g^2} \\ &= \frac{1}{8 a^2 R_c^2 B^2} \left[ \frac{A}{B} \frac{1}{j} - \frac{1}{2} \arctan \frac{A}{B j} \right] \end{aligned}$$

$$= \frac{1}{32a^2 R_c^2} \frac{T}{\hbar c} \cosh^4 \frac{E_N}{2T} W (\neq 2); \quad (\text{D } 19)$$

$$W(x) = \frac{1}{x^2 H^2(x)} \left[ 1 - \frac{Q(x)}{\hbar H(x)} - \frac{1}{2} \arctan \frac{Q(x)}{\hbar H(x)} \right] \quad (\text{D } 20)$$

Substituting this result into (D 15) and integrating the obtained  $I(\omega)$  over frequency according to (67), we arrive at Eq. (83) of the main text.

- <sup>y</sup> Also at A.F. Ioé Physico-Technical Institute, 194021 St. Petersburg, Russia.
- <sup>z</sup> Also at Petersburg Nuclear Physics Institute, 188350 St. Petersburg, Russia.
- <sup>1</sup> T.J. Gramila, J.P. Eisenstein, A.H. MacDonald, L.N. Pfeiffer, and K.W. West, Phys. Rev. Lett. 66, 1216 (1991); Phys. Rev. B 47, 12957 (1993).
- <sup>2</sup> U. Sivan, P.M. Solomon, and H. Shtrikman, Phys. Rev. Lett. 68, 1196 (1992).
- <sup>3</sup> N.P.R. Hill, J.T. Nicholls, E.H. Lindell, M. Pepper, D.A. Ritchie, A.R. Hamilton, and G.A.C. Jones, J. Phys.: Condens. Matter 8, L557 (1996).
- <sup>4</sup> H. Rubel, A. Fisher, W. Dietsche, K. von Klitzing, and K. Eberl, Phys. Rev. Lett. 78, 1763 (1997).
- <sup>5</sup> X.G. Feng, S. Zelakiewicz, H. Noh, T.J. Ragucci, and T.J. Gramila, Phys. Rev. Lett. 81, 3219 (1998).
- <sup>6</sup> M.P. Lilly, J.P. Eisenstein, L.N. Pfeiffer, and K.W. West, Phys. Rev. Lett. 80, 1714 (1998).
- <sup>7</sup> J.G.S. Lok, S.Kraus, M. Pohl, W. Dietsche, K. von Klitzing, W. Wegscheider, and M. Bichler, Phys. Rev. B 63, 041305 (2001).
- <sup>8</sup> M. Kellogg, I.B. Spielman, J.P. Eisenstein, L.N. Pfeiffer, and K.W. West, Phys. Rev. Lett. 88, 126804 (2002).
- <sup>9</sup> M. Kellogg, J.P. Eisenstein, L.N. Pfeiffer, and K.W. West, Phys. Rev. Lett. 90, 246801 (2003).
- <sup>10</sup> K.Muraki, J.G.S.Lok, S.Kraus, W. Dietsche, K. von Klitzing, D. Schuh, M. Bichler, and W. Wegscheider, cond-mat/0311151 (2003).
- <sup>11</sup> L.Zheng, and A.H. MacDonald, Phys. Rev. B 48, 8203 (1993).
- <sup>12</sup> M.C. Binsager, K. Flensberg, B.Y. Hu, and A.-P. Jauho, Phys. Rev. Lett. 77, 1366 (1996); Phys. Rev. B 56, 10314 (1997).
- <sup>13</sup> A.V. Khaetskii and Yu.V. Nazarov, Phys. Rev. B 59, 7551 (1999).
- <sup>14</sup> F. von Oppen, S.H. Simon, and A. Stem, Phys. Rev. Lett. 87, 106803 (2001).
- <sup>15</sup> A. Kamenev and Y. Oreg, Phys. Rev. B 52, 7516 (1995).
- <sup>16</sup> K. Flensberg, B.Y. Hu, A.-P. Jauho, and J.M. Kinaret, Phys. Rev. B 52, 14761 (1995).
- <sup>17</sup> T. Ando and Y. Uemura, J. Phys. Soc. Jpn. 36, 959 (1974); T. Ando, *ibid* 37, 1233 (1974).
- <sup>18</sup> K.A. Benedict and J.T. Chalker, J. Phys. C 19, 3587 (1986). For a finite correlation length  $d$  of disorder, the SCBA is justified under the condition  $\hbar v_F/d \ll \omega$ , see M.E. Raikh and T.V. Shahbazyan, Phys. Rev. B 47, 1522 (1993); B. Laikhtman and E.L. Aitshuler, Ann. Phys. 232, 332 (1994).
- <sup>19</sup> I.V. Gomyi, A.D. Mirlin, and F. von Oppen, unpublished.
- <sup>20</sup> B.N. Narozhny, I.L. Aleiner, and A. Stem, Phys. Rev. Lett. 86, 3610 (2001).
- <sup>21</sup> We remark that it was erroneously claimed in Ref. 12 that the vertex corrections are negligible for  $n \notin n^0$ .
- <sup>22</sup> Keeping the LL indices in scalar vertex corrections, it can be checked that the factor  $\text{Re} [ \chi^+(q;!) \chi^{++}(q;!)]$  in Eq. (28) involves only the vertex corrections of type  $\chi_{N,N-1}$ . Therefore, neglecting such vertex corrections<sup>21</sup> one loses the leading term (28).
- <sup>23</sup> I.L. Aleiner and L. Glazman, Phys. Rev. B 52, 11296 (1995).
- <sup>24</sup> M.G. Vavilov and I.L. Aleiner, Phys. Rev. B 69, 035303 (2004).
- <sup>25</sup> Though the theoretically predicted<sup>26,27,28</sup> anomalous  $T^{4=3}$  dependence of  $\chi_{xx}^D$  at half-filling of the lowest LL is reasonably well confirmed by the experimental data<sup>6,10</sup> for the weak-coupling regime, the observed<sup>6</sup> dependence of the drag on the magnetic field around the half-filling seems to disagree strongly with theory.
- <sup>26</sup> I. Usishkin and A. Stem, Phys. Rev. B 56, 4013 (1997).
- <sup>27</sup> S. Sakhi, Phys. Rev. B 56, 4098 (1997).
- <sup>28</sup> Y.-B. Kim and A.J.M. Illis, Physica E (Amsterdam) 4, 171 (1999).
- <sup>29</sup> The Coulomb drag at the quantum Hall transition was considered in E. Shimshoni and S.L. Sondhi, Phys. Rev. B 49, 11484 (1994). However, this work suffers from the same deficiency as Refs. 12,13: its starting point is a formula for drag which misses the contributions related to particle-hole asymmetry induced by magnetic field.